Design, Control, and Validation of a Novel Cable-Driven Series Elastic Actuation System for a Flexible and Portable Back-Support Exoskeleton

Hongpeng Liao, Hugo Hung-tin Chan, Gaoyu Liu, Xuan Zhao, Fei Gao, Masayoshi Tomizuka, *Life Fellow, IEEE*, and Wei-Hsin Liao, *Senior Member, IEEE*

***Abstract*—Various active back-support exoskeletons have been developed to assist manual materials handling work for low back injury prevention. Existing back-support exoskeleton actuation either suffers from rigid transmission structure, or fails to efficiently generate assistance via portable actuation system with flexible transmissions. In this article, a novel cable-driven series elastic actuation (CSEA) system is proposed to realize a flexible and portable back-support exoskeleton design with safe, efficient, and sufficient assistive torque output capability. The CSEA system realizes a flexible actuation based on cable transmission for an ergonomic human–exoskeleton interaction. Based on a torsion spring–support beam mechanism, it achieves an efficient assistance output capability to prevent high cable force demand and resultant lumbar compression, assuring a safe and synergistic operation for flexible exoskeleton actuation. Meanwhile, this mechanism enables the CSEA system to integrate series elastic actuator (SEA) with cable transmission and operates with multiple statuses to leverage SEA advantages and to overcome its torque output limitation. Dynamic model is established for the CSEA system, and a unified torque controller is designed for stable, continuous, and accurate torque control of the CSEA system despite its discontinuous dynamics during operation status transition. The efficacy of the closed-loop CSEA system to enable an ergonomic and efficient back-support exoskeleton actuation with the capability of accurately delivering desired level of assistance is verified via bench tests and human tests. Results verified that the CSEA system actuated exoskeleton can effectively reduce activity of relevant muscles during trunk flexion and extension motions compared to no exoskeleton case, validating successful application of the CSEA system on the exoskeleton for an effective back support effect.**

***Index Terms*—Back-support exoskeleton, cable-driven actuation, continuous tracking control, multiple status transition, series elastic actuator (SEA).**

Manuscript received 4 November 2023; revised 9 February 2024; accepted 10 March 2024. Date of publication 25 March 2024; date of current version 6 May 2024. This paper was recommended for publication by Associate Editor H. Zhao and Editor K. Mombaur upon evaluation of the reviewers' comments. This work was supported by the Hong Kong Centre for Logistics Robotics of InnoHK and Science, Technology, and Innovation Commission of Shenzhen Municipality, China, under Grant SGDX20220530111005036. An earlier version of this paper was presented in part at the 2021 IEEE International Conference on Mechatronics and Automation (ICMA), 2021 [DOI: 10.1109/ICMA52036.2021.9512715]. *(Corresponding authors: Fei Gao; Wei-Hsin Liao.)*

This work involved human subjects or animals in its research. Approval of all ethical and experimental procedures and protocols was granted by Joint Chinese University of Hong Kong –New Territories East Cluster Clinical Research Ethics Committee (Joint CUHK-NTEC CREC) under Application No. 2015.262.

Hongpeng Liao, Hugo Hung-tin Chan, Gaoyu Liu, Xuan Zhao, and Wei-Hsin Liao are with the Department of Mechanical and Automation Engineering, The Chinese University of Hong Kong, Hong Kong (e-mail: hpliao@mae.cuhk.edu.hk; htchan@mae.cuhk.edu.hk; geniuslgy0909@gmail.com; zhaoxuan505@163.com; whliao@cuhk.edu.hk).

Fei Gao is with the Shenzhen Institute of Advanced Technology, Chinese Academy of Sciences, Shenzhen 518055, China (e-mail: fei.gao@siat.ac.cn).

Masayoshi Tomizuka is with the Department of Mechanical Engineering, University of California, Berkeley, CA 94720 USA (e-mail: tomizuka@berkeley.edu).

This article has supplementary downloadable material available at https://doi.org/10.1109/TRO.2024.3381556, provided by the authors.

Digital Object Identifier 10.1109/TRO.2024.3381556

I. Introduction

MANY occupations related to industry, agriculture, and logistic demand frequent manual materials handling (MMH) work. During forward trunk bending in the MMH work, the large forces from back muscles to maintain a stable and consistent human motion dynamics can result in high physical stress on the lumbar spine [1], exposing workers to a high risk of low back injury [2]. Wearable back-support exoskeletons, which combine human flexibility and assistance from robotic system, are regarded as a promising approach to provide low back support in different scenarios [3].

Existing back-support exoskeletons are commonly equipped with rigid actuation systems that interact with the wearer through rigid structures [4], [5]. By transmitting force perpendicular to the wearer's trunk and thighs, the rigid actuation systems can effectively generate assistive torque to assist motion of hip joints as well as the spinal joints. However, rigidity of the transmission structures can restrict human natural movements and lead to misalignment between the structures and attached human body, causing safety hazards and discomfort for human–exoskeleton interaction (HEI) [6], [7], [8], [9], [10], [11], [12], [13]. The rigid actuation system commonly relies on extra mechanisms to compensate the misalignment and mitigate limitations on wearers' range of motion (RoM), bringing bulky and complex system structures [14], [15]. In contrast, the cable-driven actuation system can realize flexible actuation to avoid these limitations. It interacts with wearers via only soft cable and interaction accessories to reduce restriction on human natural RoM. Meanwhile, it can compensate misalignment between transmission structures and human body with redundant degree-of-freedoms (DoFs) from the cable transmission for an ergonomic HEI. Due to these advantages, it has been widely applied to different exoskeletons [16], [17], [18]. By leveraging flexibility of the

cable transmission, the actuation unit placement in cable-driven exoskeletons can be customized with an off-board or on-board configuration to suit the specific application requirements. To avoid large stress on exoskeleton structure and human body from large cable force, some cable-driven exoskeletons for rehabilitation and mobility enhancement place the actuation units on external frames [19], [20], [21], [22]. With the off-board actuation unit and cable route placement, these cable-driven actuation systems can easily achieve a large moment arm for the assistive force to efficiently generate sufficient assistive torque with small cable force. However, it severely hinders the exoskeleton portability. Cable-driven actuation system has also been applied with on-board actuation unit for portable exoskeletons, such as walking assistance exoskeletons [23], [24], [25], but the assistive torque output range is commonly limited by the small moment arm relative to the assisted human joints.

Considering the challenging requirements of portability and high assistance output, few back-support exoskeletons were equipped with cable-driven actuation systems [4]. Yang et al. [26] applied cable-driven actuation for a continuum soft back-support exoskeleton but with an off-board actuation unit. In [27], [28], and [29], portable cable-driven back-support exoskeletons were developed to assist symmetric trunk flexion and extension (TFE) motion. Li et al. [30] designed a cable-driven back exosuit to provide assistance for both symmetric and asymmetric TFE motion. Based on the cable-driven actuation system, these back-support exoskeletons achieved a flexible exoskeleton design to interact with wearers' trunk via soft structures. These conventional cable-driven actuation systems placed the cable behind and parallel to the human trunk. Compared with biological back muscles, they keep mechanical advantages to support for TFE motion via lower forces with a larger moment arm relative to hip and spinal joints. However, the moment arm remains much lower than that of rigid actuation systems, setting a higher force demand to output same assistive torque. In comparison to the rigid actuation systems, the parallel cable placement and high cable force demand of the conventional cable-driven actuation system result in a relative inefficient assistance output capability, both mechanically and biomechanically. From the mechanical design aspect, the high cable force required to generate assistive torque can put large stress on the exoskeleton structure, leading to operation safety risks in the case of structural fracture. Meanwhile, a high-power actuation unit to meet the high cable force demand can bring heavy weight and high output impedance. From the biomechanical aspect, the parallel assistive force on human trunk could result in lumbar compression similar as back muscle forces to weaken the assistive effect on lumbar loads alleviation [15], [31]. Moreover, uncomfortable HEI may be induced from a large interaction force exceeding certain comfort limits [32].

In addition to cable transmissions, compliant actuators are also commonly adopted to improve exoskeleton actuation performance and HEI experience [33]. Among them, series elastic actuator (SEA), which incorporates series elasticity between the actuation unit output and load side [34], is widely applied to reduce actuation output impedance and improve force controllability, shock tolerance, and HEI safety [35], [36]. Some exoskeleton actuation systems combine SEA with cable transmissions to empowered cable-driven actuation with SEA features [37], [38], [39], [40]. For back-support exoskeleton, Hyun et al. [11] and Lee and Kim [12] applied SEA with cable transmissions to achieve an energy efficient exoskeleton actuation while the transmission structure remains rigid. In contrast, while Song et al. [29] integrated SEA into a flexible cable-driven actuation, the force transmission follows the conventional parallel placement with a relatively inefficient assistance output capability.

As the SEA characteristics are largely affected by the stiffness of the serial elastic component, the application of SEAs is also limited with performance tradeoffs brought by different selections of the serial elastic component [41], [42]. Specifically, SEAs with low stiffness elastic component can obtain high compliance and shock tolerance, benefiting for smooth and safe force control, but have a narrow force bandwidth. Moreover, the low stiffness and finite deflection of the elastic component would limit the SEA force output range, as reported in [11], [12], and [29]. By contrast, SEAs with high stiffness elastic component can output large force with a wide force control bandwidth but at the expense of low force output fidelity and high output impedance. In order to better leverage SEA advantages and avoid its limitations, SEAs with adjustable stiffness have been investigated [43], [44]. However, these variable stiffness systems are usually highly complex, heavy, and bulky, limiting the application for portable exoskeleton actuation. In this article, based on a compact torsion spring–support beam mechanism with deflection constraint, a cable-driven series elastic actuation (CSEA) system is developed to operate with two statuses to gain SEA features while overcoming its limitations. With freely deflected torsion springs under a small assistive torque output, the CSEA system performs with dynamics as a SEA, which is defined as SEA status. When the torsion springs are constrained from deflection under a large torque output, the CSEA system would transit to operate with dynamics as a conventional stiff actuator (CSA) to overcome the output limitations of SEA status for fast and sufficient assistive torque output. This operation status is defined as CSA status.

The transition of the operation status can lead to a discontinuous system dynamics, making it challenging to achieve a stable, continuous, and accurate torque tracking. Specifically, various control methods have been developed for force control of CSAs [45], [46], [47] and SEAs with constant stiffness or variable stiffness [48], [49], [50], [51]. For a SEA with multistage stiffness, Yu et al. [52] designed a switching controller for force control of a SEA with two-stage stiffness and Li et al. [53] designed a continuous controller for position control of the same SEA. However, these controllers do not provide direct solutions to ensure a desired stable, continuous, and accurate torque control of actuation systems capable of transitioning between SEA status and CSA status in which the interface between actuation unit output and its load is highly stiff, contrasting with the compliant interface of SEA status.

The goal of this article is to develop an actuation system to facilitate a flexible and portable back-support exoskeleton design to generate sufficient assistive torque ergonomically and efficiently. To this end, this article presents the design, control, and validation of a novel CSEA system. First, a novel CSEA system with multiple operation statuses is developed to realize a flexible and compliant back-support exoskeleton actuation with an efficient assistance output capability. Second, dynamic models are established to describe the CSEA system dynamics in different operation status. Third, a unified torque controller is designed to ensure a stable, continuous, and accurate torque control of the CSEA system. The stability of the closed-loop system is theoretically analyzed. Finally, both bench tests and human tests are carried out to validate the effectiveness of the closed-loop CSEA system for back-support exoskeleton application.

The core contributions of this article lie in the improvements of the proposed CSEA system over conventional cable-driven back-support actuation systems and the proposal of the unified torque controller.

1) Instead of placing the cable parallel to the wearer's trunk as the conventional cable-driven actuation systems, the CSEA system connects the cable to the human trunk with an interaction angle for a bias force output using a support beam. It effectively enlarges the moment arm of the transmitted cable force and reduces the force parallel to the wearer's trunk, enhancing the assistance output efficiency both mechanically and biomechanically.
2) The CSEA system enhances cable-driven actuation with SEA advantages compared with the actuation systems in [26], [27], [28], and [30], and operates with multiple statuses to overcome torque output limitations of SEA mentioned in [11], [12], and [29], realizing a flexible and compliant back-support exoskeleton actuation with a large assistance output capability.
3) A unified torque controller is designed and validated to ensure a stable, continuous, and accurate torque control for the actuation system with operation status transitioning between SEA status and CSA status like the proposed CSEA system, which cannot be directly achieved by the existing force controllers for CSAs or SEAs with fixed or variable stiffness.

This article extensively extends our previously work in [54] in the following aspects:

1) design of a compact torsion spring–support beam mechanism with deflection constraint to enable the CSEA system to operate with multiple statuses to gain SEA features while overcoming torque output limitations of SEA;
2) modeling of kinematics and dynamics of the CSEA system;
3) analysis of operation principle and output capability of the CSEA system, based on which its design guidelines are summarized for practical implementation;
4) development of a unified torque controller for stable, continuous, and accurate torque control of the CSEA system with sound stability proof;
5) implementation of the CSEA system for a flexible and portable back-support exoskeleton;
6) efficacy validation of the CSEA system and the unified torque controller via bench tests and human tests.

TABLE I
PARAMETERS OF THE BACK-SUPPORT EXOSKELETON ACTUATION SYSTEM

Parameters	Desired	CSEA System
Max. assistive torque output (N·m)	> 50	75
Max. adapted TFE speed (rad/s)	> 2	2.42
Force on shoulder under 50 N·m assistive torque output (N)	< 310.5	130
Assistive torque bandwidth (Hz)[#]	> 0.5	3.65
Resistance on unassisted motion (N·m)[#]	0	0.2
RoM reduction of trunk flexion[*] (° / % relative to natural RoM)	0 / 0	5.1°/4.0%
RoM reduction of trunk lateral bending[*] (° / % relative to natural RoM)	0 / 0	2.5°/4.8%
RoM reduction of trunk axial rotation[*] (° / % relative to natural RoM)	0 / 0	0.3°/0.6%

[#] tested for the closed-loop CSEA system.
[*] tested for the CSEA exoskeleton equipped with two CSEA systems.

The rest of this article is organized as follows. Section II details the CSEA system, including the design requirement, system architecture, working principle and output capability. Section III establishes the CSEA system model. Section IV describes the unified torque controller. Section V evaluates performance of the closed-loop CSEA system via experiments. Discussions are presented in Section VI. Finally Section VII concludes this article.

II. CSEA System Design

A. Design Requirements

To achieve an ergonomic and effective assistance of TFE, the back-support exoskeleton actuation system is expected to the following:

1) put no restriction on natural RoM and render zero output impedance to unassisted movements;
2) ergonomically transmit assistive torque for a safe and comfortable HEI;
3) timely, accurately, and smoothly output sufficient assistive torque for effective assistance.

Specifically, as listed in Table I, the actuation system should not only accommodate the TFE motion in the sagittal plane, but also the trunk lateral bending in the frontal plane and axial rotation in the transverse plane to preserve a natural trunk RoM. Moreover, resistive torque from the actuation system is desired to be zero during the movements other than the target-assisted TFE motion to avoid undesired resistance.

For the second expectation, the actuation system should have sufficient DoFs to compensate misalignments between actuated exoskeleton joint and assisted human joints. This is to avoid parasitic forces and relative movement between the interaction attachment and the human trunk for an ergonomic assistance transmission. It is additionally desired that the force acting on human trunk from the auction system should stays blow the

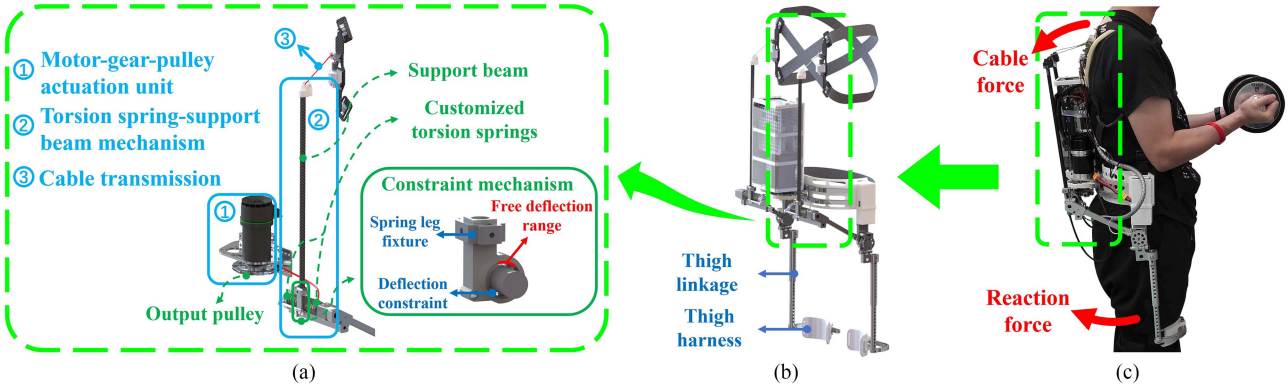

Fig. 1. Architecture of the CSEA system and its implementation on a flexible and portable back-support exoskeleton. (a) CSEA system architecture. (b) CAD model of the back-support exoskeleton with two CSEA systems (CSEA exoskeleton). (c) Subject wearing the CSEA exoskeleton prototype.

comfort limit of 310.5 N per shoulder [32] to guarantee a safe and comfortable HEI as listed in Table I.

The requirements to meet the third output expectation are specified based on the biomechanical characteristics of TFE motion, as listed in Table I. According to previous studies [55], [56], a peak biological moment about 200 N·m can be generated on hip and lumbar spinal joints under a peak trunk flexion velocity of around 2 rad/s during common TFE motions. To meet the third expectation, the back-support exoskeleton is expected to be capable of generating an assistive torque exceeding half the peak biological moment to keep the potential for providing sufficient assistance for different TFE motions. Assuming that the back-support exoskeleton is powered by two actuation systems, each actuation system is thus required to be able to output an assistive torque of over 50 N·m. Meanwhile, it is required to be able to deliver the peak assistive torque under the TFE motion speed of 2 rad/s to avoid being speed limited. To better ensure a timely and accurately assistive torque delivery for assisting TFE at various speeds and frequencies, the actuation system is required to achieve a torque bandwidth of no less than 0.5 Hz, which is double of the maximum recommended continuous lifting frequency (15 lifts/min) [57].

B. System Architecture and Rationale

The CSEA system and a flexible and portable back-support exoskeleton adapted from [56] called CSEA exoskeleton, which is equipped with two CSEA systems, are shown in Fig. 1. Each CSEA system consists of a motor–gear–pulley actuation unit, a cable transmission, and a torsion spring–support beam mechanism, which is comprised of a support beam and a torsion spring set with deflection constraint. The force from the actuation unit is transmitted to human trunk through the cable transmission. With the hip joint clutched with thigh assembly during exoskeleton operation, the reaction force on the torsion spring set is transmitted to the thigh via the thigh linkage and harness. These force transmissions work in conjunction to generate assistive torque on hip and lumbosacral (L5/S1) joints for TFE assistance, as depicted in Fig. 1(c). With the flexibility of the cable, the CSEA system interacts with human trunk through only soft structure. Rather than being placed parallel to human trunk, the cable out from the actuation unit is guided through the support beam before connected to human trunk for a bias cable force. As a result, the moment arm of the cable force relative to lumbosacral joint is effectively enlarged compared with the conventional cable-driven actuation system. Within the torsion spring–support beam mechanism, the base of the support beam is connected to the torsion spring set. The spring set consists of two torsion springs for the convenience of adjusting stiffness by setting different spring combinations. Meanwhile, a constraint mechanism is set to impose a constraint to the torsion spring deflection to enable the CSEA system operates with multiple statuses. Specifically, it operates in SEA status when the torsion springs were deflected within the free deflection range. After the torsion springs encounter the constraint under a sufficient large assistive torque output, the CSEA system operates in CSA status. In SEA status, the torsion springs and support beam would rotate under transmission of varying levels of assistive torque. The elasticity of the torsion springs enables the CSEA system to perform as a SEA with intrinsic compliance. In CSA status, the torsion springs are constrained from rotating in response to assistive torque variation due to the imposed deflection constraint. The CSEA system directly transmits cable force to human trunk without deflecting any elastic component as a CSA.

The schematic diagrams of the CSEA system operating in SEA status and CSA status are shown in Fig. 2. The gray link with length of D represents the human trunk. The red link with length L refers to the support beam connected to the torsion spring set with equivalent stiffness k, which is illustrated by a spiral. The blue line with length l linking the human trunk and the support beam tip denotes the taut cable during the CSEA system operation. The initial angle θ_0 denotes the intersection angle between the support beam and human trunk that initially leads to a taut cable when the exoskeleton wearer starts to flex the trunk. θ_c denotes the allowable deflection angle of the torsion springs before reaching the deflection constraint. The rotation axis of the torsion spring set, i.e., support beam rotation axis, is assumed to coincide with the equivalent axis of the hip and lumbosacral joint rotation for the simplification of the kinematics and kinetics

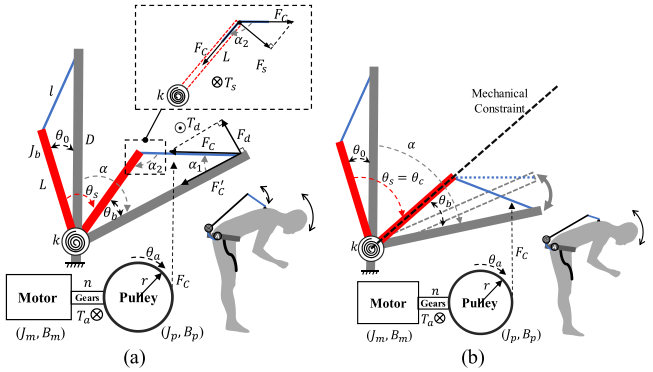

Fig. 2. Schematic diagram of the CSEA system. (a) SEA status. (b) CSA status.

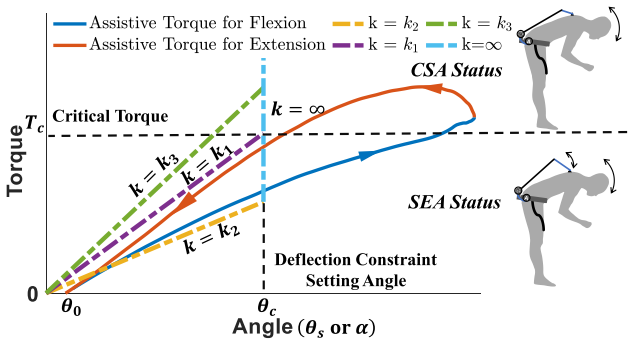

Fig. 3. Representative assistive torque–human trunk flexion angle profile whose horizontal axis is α and torque–rotation characteristic of the support beam whose horizontal axis is θ_s.

analysis. The reasonability of this assumption with minor effect on the accuracy of the kinematics and dynamics modeling is verified through experiments presented in Section V. With this assumption, a triangular configuration is formed by the support beam, human trunk, and the taut cable during the CSEA system operation. Based on this kinematics geometry, the delivered assistive torque T_d from the cable force F_c for TFE assistance can be calculated as

$$T_d = F_d \cdot D = F_c \cdot \sin(\alpha_1) \cdot D \tag{1}$$

where F_d is the perpendicular component of F_c relative to human trunk, and α_1 is the angle between the taut cable and human trunk.

As shown in Fig. 2(a), due to the perpendicular component force F_s on the tip of the support beam, the support beam would rotate with the torsion springs for an angle θ_s in SEA status. The resultant torque T_s, which induces a deflection of θ_s for the torsion springs, can be calculated as

$$T_s = F_s \cdot L = F_c \cdot \sin(\alpha_2) \cdot L = k \cdot \theta_s \tag{2}$$

where α_2 denotes the angle between the support beam and the taut cable.

For the triangular system configuration, the following relationship can be obtained from law of sine:

$$D \cdot \sin(\alpha_1) = L \cdot \sin(\alpha_2). \tag{3}$$

Based on (1)–(3), relation between the assistive torque T_d and the spring deflection θ_s in SEA status is given by

$$T_d = T_s = k \cdot \theta_s. \tag{4}$$

This enables the CSEA system to obtain the assistive torque feedback from spring deflection, such as conventional SEAs. In the SEA status, the CSEA system operates with similar dynamics and features as conventional SEA, including the torque feedback capability and intrinsic compliance. This is theoretically validated via the model established in Section III.

When the generated cable force increases to output an assistive torque exceeding the critical torque T_c ($k \cdot \theta_c$), the deflection constraint would hold the torsion springs and support beam to prevent further deflection. The CSEA system would thus operate as a CSA, as illustrated in Fig. 2(b). In this CSA status, the delivered assistive torque can be calculated based on cable force F_c following the definition (1) as:

$$\begin{aligned} T_d &= F_c \cdot \sin(\alpha_1) \cdot D \\ &= F_c \cdot \frac{L}{\sqrt{L^2 + D^2 - 2 \cdot L \cdot D \cdot \cos(\theta_b)}} \cdot \sin(\theta_b) \cdot D \end{aligned} \tag{5}$$

where θ_b denotes the angle between the support beam and human trunk, which is given by

$$\theta_b = \theta_0 + \alpha - \theta_s \tag{6}$$

where α denotes the human trunk flexion angle.

It should be noted that the positive directions of T_s, T_d, θ_s, and α follow the indication as shown in Fig. 2.

C. System Structural Specifications Determination and Operation Process Analysis

The CSEA system structural specifications, including torsion spring set stiffness k, deflection constraint setting angle θ_c, and support beam length L, are determined to ensure an effective and efficient assistive torque generation. A representative assistive torque profile relative to trunk flexion angle is plotted in Fig. 3 based on collected human TFE motion data [54]. This profile captures the characteristics of commonly applied assistive strategies, which produce lower assistive torque during trunk flexion motion for less hindrance and larger assistive torque during trunk extension motion for sufficient assistance [5], [11], [29], [58]. It should be noted that the zero-reference point in the horizontal axis is set as the initial tilt angle of the support beam. The torque–rotation characteristic of the support beam is also plotted in Fig. 3. In SEA status, it is equivalent to that of the torsion spring set, presented as a straight line with slope of k. After the torsion springs reach the deflection constraint at θ_c, the characteristic profile of the support beam turns to a vertical line with an infinite slope. According to the assistive torque definition (1), to guarantee a successful CSEA system operation, a positive intersection angle between cable and human trunk should be maintained, i.e., a positive θ_b and α_1. This is achieved by determining an appropriate torsion spring set stiffness k to

TABLE II
CSEA SYSTEM SPECIFICATIONS FOR IMPLEMENTATION ON THE CSEA EXOSKELETON

Item		Specifications
Cable		7×19 stainless steel wire; Diameter: 1.5 mm
Torsion Spring-Support Beam Mechanism	Torsion spring set	Stiffness: 0.52 N·m/° Maximum safe deflection: 54.55°
	Support beam	Length: 75% of the weaer's trunk length
Actuation unit	Pulley	Radius: 0.05 m
	Gearbox	Maxon GP52C; Reduction ratio: 19:1
	Motor	Maxon EC60-614949; Rated Power: 200 W Nominal torque: 0.536 N·m Nominal speed: 3240 r/min
Motor driver		Maxon ESCON 70/10

ensure no intersection between the support beam characteristic profile and the assistive torque profile.

As illustrated in Fig. 3, a small stiffness k_2 leads to an intersection between the characteristic profile of the support beam and the assistive torque profile. With large stiffness, such as k_3, while a positive θ_b and α_1 is achieved, it can lead to a support beam characteristic profile deviating far from the assistive torque profile, resulting in an obtrusive support beam lagging the human trunk with a large intersection angle θ_b. It can also weaken the ability to achieve a smooth force control and low output impedance. Instead, the torsion spring set stiffness should be set close to the rendered stiffness of the assistive torque profile like k_1 for which a positive θ_b and α_1 are assured while avoiding obtrusive lag of the support beam. On the other hand, the deflection constraint setting angle θ_c should be set at an angle below the maximum safe deflection of the applied torsion springs. The angle is then set at a specific angle under consideration to properly transition the CSEA system to operate in CSA status when there is an expected demand of large and rapid increasing assistance. There considerations are to overcome limitations of SEAs on torque output range and bandwidth. For the support beam, while a longer beam can generally lead to an increased moment arm with a larger α_1 for a higher assistive torque output efficiency as indicated, it increases the obtrusiveness behind the wearer. Therefore, a balance between assistive torque output efficiency and the compactness of the CSEA system is required.

Based on these considerations, the structural specifications of the CSEA system equipped by the CSEA exoskeleton are determined, as listed in Table II. According to the requirements in Section II-A, the desired maximum assistive torque output from each CSEA system is 50 N·m. Assuming that this peak assistance demand occurs at a trunk flexion angle of 90° to 100°, the assistive torque profile renders an overall stiffness around 0.52 N·m/° relative to the trunk flexion angle. Hence, the stiffness of the torsion spring set is determined as 0.52 N·m/° to guarantee a successful and low-profile operation of the CSEA system with a proper positive θ_b. The deflection constraint setting angle can be adjusted below the maximum safe deflection of the applied torsion springs (54.55°). The support beam length L is set as 75% of the wearer's trunk length D, which can guarantee an average force moment arm being 70.3% of D as calculated based on (5), for an efficient assistive torque generation.

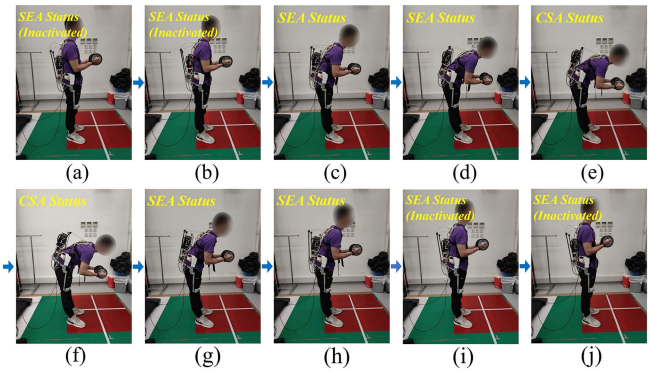

Fig. 4. Demonstration of the CSEA system operation process during implementation of CSEA exoskeleton for one cycle of TFE assistance. (a) and (b) CSEA system is inactivated during early trunk flexion phase. (c) and (d) CSEA system operates in SEA status. (e) and (f) CSEA system operates in CSA status, (g) and (h) CSEA system operates in SEA status. (i) and (j) CSEA system is inactivated during late trunk extension phase.

With the specifications listed in Table II, the operation process of the CSEA system is demonstrated in Fig. 4. As shown in Fig. 4(a) and (b), in the early trunk flexion phase with a small flexion angle, the cable is slack and the CSEA system is inactive. This is to avoid restricting and impeding of unassisted motions with slight trunk flexion motion, such as walking. When the wearer starts to flex the trunk to a position where the intersection angle θ_b between support beam and the trunk reaches θ_0, the CSEA system is activated to operate in SEA status, as shown in Fig. 4(c) and (d). Under a high assistance demand of the TFE motion with a large flexion angle, the CSEA system would transition from operating in SEA status to CSA status to output a large assistive torque exceeding the critical torque T_c, as shown Fig. 4(e) and (f). As the assistive torque falls below T_c along with trunk extension, the CSEA system transitions back to operate in SEA status, as depicted in Fig. 4(g) and (h). Finally, as the wearer extends the trunk to erect posture with no assistance demand, the CSEA system is inactivated again, as illustrated in Fig. 4(i) and (j).

D. Actuation Unit Determination

First, the output pulley radius, r, is set as 0.05 m to ensure an efficient cable force output while providing sufficient cable bending radius and avoiding extra cable windings. Based on this, the required actuation unit specification to generate the targeted 50 N·m at 2 rad/s of TFE motion is calculated. The required actuation unit output torque and velocity to satisfy the output requirements are then calculated for reference of determining the motor and gearbox. Based on (5), the cable force for a 50 N·m assistive torque output under different CSEA system configurations can be calculated. The required actuation unit torque output is computed by multiplying the required cable force by the output pulley radius r. Based on the law of cosine, the kinematics relationship of the angular position of the actuation unit output pulley θ_a, the intersection angle θ_b, and the taut cable length l is given by

$$l = l_0 - \theta_a \cdot r = \sqrt{L^2 + D^2 - 2 \cdot L \cdot D \cdot \cos(\theta_b)} \quad (7)$$

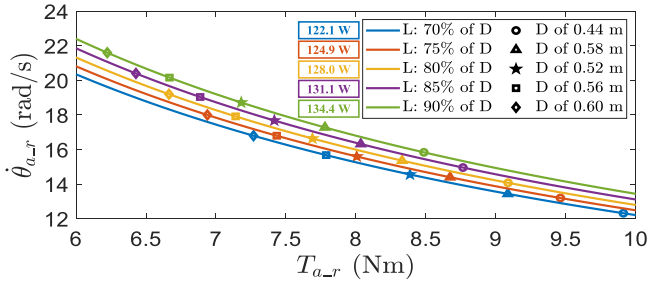

Fig. 5. Required maximum actuation unit torque output T_{a_r} for 50 N·m assistive torque output and maximum actuation unit velocity $\dot{\theta}_{a\_r}$ to keep taut cable under 2 rad/s of $\dot{\alpha}$ with output pulley radius r of 0.05 m.

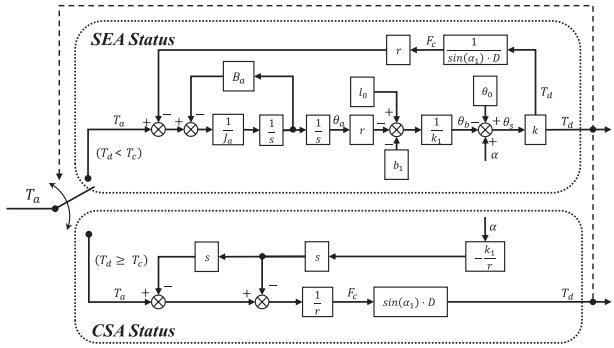

Fig. 6. Block diagram of the CSEA system model. The switch indicates that the CSEA system operates with SEA status dynamics when $T_d < T_c$ and operates with CSA status dynamics when $T_d \geq T_c$.

where l_0 is the length of a taut cable between the support beam tip and the human trunk when θ_b equals θ_0. Based on (6) and (7), the required velocity of the actuation unit output pulley to keep a tensioned cable with 2 rad/s of $\dot{\alpha}$ under different CSEA system configurations can be calculated.

For the output capability analysis, the intersection angle θ_b between the support beam and human trunk is assumed to vary within 20°–90°. The support beam length L is set as 70%–90% of trunk length D, which is set from 0.44 to 0.60 m to represent the trunk length range of an average person. With $r = 0.05$ m, the required maximum actuation unit torque output T_{a_r} to output a 50-N·m assistive torque, and the required maximum actuation unit output pulley velocity $\dot{\theta}_{a\_r}$ to keep a tensioned cable with 2 rad/s of $\dot{\alpha}$ for CSEA system are calculated and plotted in Fig. 5. For the calculation of $\dot{\theta}_{a\_r}$, the CSEA system is expected to operate in CSA status with a zero $\dot{\theta}_s$ under the large assistive torque output of 50 N·m. As depicted, the required power of the actuation unit varies from 122.1 to 134.4 W depending on the scaled support beam length L. Hence, with a determined scaled L, the actuation unit with rated power larger than the corresponding maximum power consumption can satisfy the output requirements. In fact, the $\dot{\theta}_{a\_r}$ and the T_{a_r} will not occur simultaneously as they correspond to CSEA system configuration with different θ_b, leading to a maximum power demand looser than the analyzed results. Therefore, an actuation unit selected based on this analysis can robustly guarantee an output capability of the CSEA system surpassing the requirement.

Based on above analysis, the motor and gearbox are selected, as listed in Table II. With a rated power of 200 W, the selected motor and gearbox can power the actuation unit to output a torque of 10.18 N·m at a speed of 17.86 rad/s. The applied actuation unit thus sufficiently covers the requirements for the CSEA system with scaled L being 75% of D indicated in Fig. 5. As a result, considering a wearer with an average trunk length D of 0.492 m for a Chinese adult [59], [60], the CSEA system with specifications listed in Table II can output a maximum assistive torque of over 75 N·m under a TFE motion speed of 2.42 rad/s, sufficiently fulfilling the requirements, as listed in Table I.

III. CSEA System Modeling

Dynamic models are established for the two operation statuses of the CSEA system. Fig. 6 shows the block diagram of the established CSEA system model.

A. Modeling of SEA Status

In the SEA status, the motor–gear–pulley actuation unit dynamics and support beam dynamics are described by

$$J_a \cdot \ddot{\theta}_a + B_a \cdot \dot{\theta}_a = T_a - F_c \cdot r \tag{8}$$

$$J_b \cdot \ddot{\theta}_s = T_s - k \cdot \theta_s \tag{9}$$

where $J_a = (n^2 \cdot J_m + J_p)$, $B_a = (n^2 \cdot B_m + B_p)$, θ_a is the angular position of the actuation unit output pulley, and $\dot{\theta}_a$ and $\ddot{\theta}_a$ denote its angular velocity and acceleration, respectively. T_a denotes the input torque from the actuation unit. The positive direction of T_a and θ_a are defined as the direction leading to a pulling cable force. θ_s denotes the angular position of the support beam and $\ddot{\theta}_s$ denotes its angular acceleration. J_m and B_m denote the rotary inertia and damping factor of the motor. J_p and B_p denote the lumped rotary inertia and damping factor of the gearbox and the pulley within the actuation unit. n is the reduction ratio of the gearbox. J_b represents the rotary inertia of the support beam. Considering that the support beam should be lightweight with a small J_b, the inertia term in (9) is thus omitted. Hence, the dynamic assistive torque transmission is assumed to follow the identical relationship of the static condition expressed as (1)–(4), for which the reasonability is verified via torque tracking control tests in Section V.

The cable length l varies with the intersection angle θ_b as expressed in (7). The variation of l in relation to θ_b presents a high linearity. To illustrate the linearity, variation of l with θ_b varying from 20° to 90° and its corresponding linear regression are calculated for scale L from 40% to 90% of trunk length D, which is assumed as 0.492 m. As shown in Fig. 7, the coefficient of determination R^2 of the linear regressions is larger than 0.997, indicating a highly linear relationship between l and θ_b.

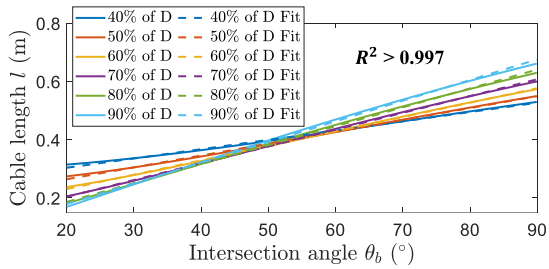

Fig. 7. Variation of the cable length l with intersection angle θ_b between support beam and human trunk and its corresponding linear regression. The calculations are conducted with assumed trunk length D of 0.492 m.

Therefore, the relationship between l and θ_b can be approximated by a linear equation as

$$l = k_1 \cdot \theta_b + b_1 \tag{10}$$

where k_1 and b_1 are two constants specifically dependent on the support beam length L and the trunk length D.

Based on the definition (6) of θ_b, kinematics relationship (7) regarding cable length l and its linear approximation (10), the actuation unit dynamics (8) can be rewritten as

$$\left(\tfrac{k_1 \cdot J_a}{r}\right)\ddot{\theta}_s + \left(\tfrac{k_1 B_a}{r}\right)\dot{\theta}_s = T_a + \left(\tfrac{k_1 J_a}{r}\right)\ddot{\alpha} + \left(\tfrac{k_1 B_a}{r}\right)\dot{\alpha} - F_c r. \tag{11}$$

where $\dot{\alpha}$ and $\ddot{\alpha}$ are the angular velocity and acceleration of trunk flexion motion, respectively.

By substituting the torque transmission relationship of SEA status (1) and (4) into (11), the dynamic model of the CSEA system in SEA status is given by

$$J_s \ddot{T}_d + B_s \dot{T}_d + K_s T_d = T_a + F(\dot{\alpha}, \ddot{\alpha}). \tag{12}$$

where

$$\begin{cases} J_s = \frac{k_1 \cdot J_a}{k \cdot r} \\ B_s = \frac{k_1 \cdot B_a}{k \cdot r} \\ K_s = \frac{r}{\sin(\alpha_1) \cdot D} \\ F(\dot{\alpha}, \ddot{\alpha}) = \left(\frac{k_1 \cdot B_a}{r} \cdot \dot{\alpha} + \frac{k_1 \cdot J_a}{r} \cdot \ddot{\alpha}\right). \end{cases} \tag{13}$$

The block diagram of the model is illustrated as the upper part with satisfaction of condition $(T_d < T_c)$ in Fig. 6.

Remark 1: Based on the established model (12) of SEA status, it can theoretically verify that the CSEA system in SEA status has SEA features of torque feedback capability and intrinsic compliance. Specifically, the transition between (11) and (12) implies that the torque feedback capability (4) of SEA status can turn the CSEA system from a torque-controlled system to an equivalent position-controlled system. According to (12) and (13), the output impedance of the CSEA system in SEA status, which is defined as the transfer from trunk flexion angle α to resultant interaction torque T_d with actuation unit shut off ($T_a = 0$), can be derived as

$$\frac{T_d}{\alpha} = k \cdot \frac{(j\omega)^2 + \frac{B_a}{J_a} \cdot (j\omega)}{(j\omega)^2 + \frac{B_a}{J_a} \cdot (j\omega) + \frac{k \cdot r^2}{k_1 \cdot J_a \cdot \sin(\alpha_1) \cdot D}}. \tag{14}$$

Equation (14) indicates that the output impedance would approach the intrinsic stiffness k of the serial torsion springs as the load-side motion frequency tends to infinity ($\omega \to \infty$), presenting a same characteristic as common SEAs [42], [61].

B. Modeling of CSA Status

In CSA status, the actuation unit dynamics remains as (8). Meanwhile, cable length l varies with θ_b following an identical relationship to that in SEA status, as expressed in (7). Therefore, the linear approximation (10) is also valid for the CSA status. Unlike in SEA status, the support beam and torsion springs are stationary with $\theta_s = \theta_c$ and $\dot{\theta}_s = \dot{\theta}_s = 0$ due to the imposed deflection constraint. Based on (6), (7), and (10), the actuation unit dynamics (8) in CSA status can be rewritten as

$$F_c r = T_a + \left(\frac{k_1 \cdot B_a}{r}\right) \cdot \dot{\alpha} + \left(\frac{k_1 \cdot J_a}{r}\right) \cdot \ddot{\alpha}. \tag{15}$$

By substituting the torque transmission relationship of CSA status (5) into (15), the dynamic model of the CSEA system in CSA status is given by

$$K_s \cdot T_d = T_a + F(\dot{\alpha}, \ddot{\alpha}) \tag{16}$$

where K_s and $F(\dot{\alpha}, \ddot{\alpha})$ follow definitions in (13) as for SEA status. The block diagram of this model is illustrated as the lower part with satisfaction of condition $(T_d \geq T_c)$ in Fig. 6.

Remark 2: The CSA status model (16) is equivalent to the SEA status model (12) with k being infinite large, therefore allowing the torque output range of the CSEA system to not be limited by the spring deflection range in CSA status. Meanwhile, without the actuation unit inertia effect as indicated in (12), the CSEA system in CSA status can generate assistive torque with a rapid responsiveness, effectively overcoming the torque output speed limitation of SEAs. The difference between SEA status model (12) and CSA status model (16) implies that controllers designed specifically for CSA or SEA cannot explicitly guarantee a stable, continuous, and accurate control effect for the CSEA system operating with status transition between SEA status and CSA status.

IV. Unified Torque Controller Design

In this section, a unified torque controller is designed for stable, continuous, and accurate torque control of the CSEA system with multiple operation statuses. First, a status indicator P is defined as a continuous differentiable function of the delivered assistive torque T_d with a form referring to [53] to indicate the CSEA system operation status

$$P = 1 - \frac{\left\{\min\left[0, \quad \left[\min\left(0, \quad T_d^2 - T_t^2\right)\right]^2 - \left[(\lambda \cdot T_t)^2 - T_t^2\right]^2\right]\right\}^2}{\left((\lambda \cdot T_t)^2 - T_t^2\right)^4} \tag{17}$$

where $0 < \lambda < 1$ is the coefficient that determines the steep level of the transition. T_t is a coefficient to indicate the transition torque where the transition would occur.

Variation of P with T_d is illustrated in Fig. 8. P equals 1 when T_d is between 0 and $\lambda \cdot T_t$ is regarded as SEA status since the torsion springs do not reach the deflection constraint. When T_d exceeds the transition torque T_t, P equals 0 and it indicates CSA

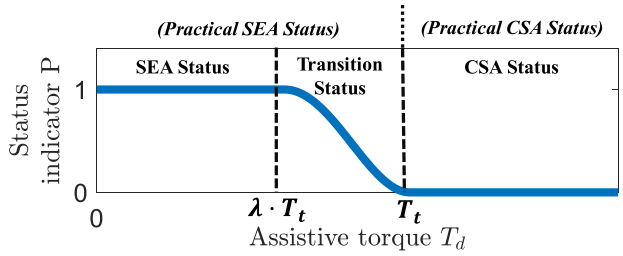

Fig. 8. Variation of status indicator P with delivered assistive torque T_d.

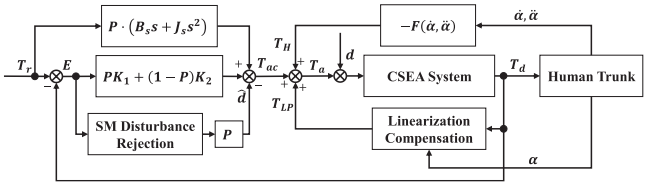

Fig. 9. Block diagram of the closed-loop CSEA system with proposed unified torque controller.

status with torsion springs encountering the constraint. When T_d varies between $\lambda \cdot T_t$ and T_t, P smoothly varies between 1 and 0 to indicate the transition between SEA status and CSA status, which is defined as transition status. It should be noted that when T_t is set smaller than the actual critical torque T_c, the CSEA system indicated in transition status would operate with SEA status dynamics with T_d being smaller than T_c, as well as T_t.

Based on (4), the feedback of the assistive torque output in SEA status with $P = 1$ can be obtained from torsion spring deflection measurement. Although the assistive torque output can also be calculated from cable force following (5), the assistive torque feedback from torsion spring deflection measurement is preferred to obtain a more accurate status indication via P as the deflection constraint is set for the torsion spring deflection. Moreover, since the torsion spring torque would not undergo potential sudden change like cable force, acquiring the feedback from torsion spring deflection measurement helps to keep a high tolerance for impacts and shocks in SEA status. In CSA status with $P = 0$, the assistive torque output is calculated based on the cable force following (5). In order to guarantee effective and continuous torque feedback when CSEA system operates with status transitions, the assistive torque output T_d is acquired by following a unified feedback law based on the status indicator P as

$$T_d = P \cdot T_{d1} + (1 - P) \cdot T_{d2} \tag{18}$$

where T_{d1} is the feedback of assistive torque output from torsion spring deflection measurement following (4) and T_{d2} is the feedback from cable force calculation following (5).

Based on the status indicator P, the unified torque controller is further designed. Fig. 9 shows the block diagram of the closed-loop CSEA system with the unified torque controller. The control law of the unified torque controller is

$$T_a = T_{LP} + T_H + T_{ac} \tag{19}$$

where T_{LP} is the linearization compensation term to compensate the nonlinear amplification coefficient K_s of the CSEA system, T_H is for human motion effect compensation, and T_{ac} is a unified feedback control term.

Specifically, T_{LP} is designed as follows:

$$T_{LP} = (K_s - K) \cdot T_d \tag{20}$$

where K_s is the nonlinear amplification coefficient expressed as (13) and K is the set nominal amplification coefficient.

Based on the model of SEA status (12) and CSA status (16), T_H is set to counteract the inertia effect from the human motion, which is given by

$$T_H = -F\ (\dot{\alpha}, \ddot{\alpha}) = -\left(\frac{k_1 \cdot B_a}{r}\dot{\alpha} + \frac{k_1 \cdot J_a}{r}\ddot{\alpha}\right). \tag{21}$$

The unified feedback control term is designed as

$$T_{ac} = P \cdot K_1 \cdot E + (1 - P) \cdot K_2 \cdot E + P \cdot \left(B_s \cdot \dot{T}_r + J_s \cdot \ddot{T}_r - \hat{d}\right) + K \cdot T_r \tag{22}$$

where T_r is the reference torque command, and $E = [e\ \ \dot{e}]^T$ denotes the torque tracking error state vector for which $e = (T_r - T_d)$. $K_1 = [k_{11}\ \ k_{12}]$ and $K_2 = [k_{21}\ \ k_{22}]$ are the feedback control gain vectors designed for SEA status and CSA status, respectively. $\hat{d}$ denotes a disturbance rejection term. Based on P, the two feedback control gain vectors are united as a unified term (22).

Based on (19) to (22), when the CSEA system operates in SEA status with $P = 1$, the control law of the unified torque controller is given by

$$T_a = T_{LP} + T_H + K_1 E + B_s \dot{T}_r + J_s \ddot{T}_r + K T_r - \hat{d} \tag{23}$$

which shows that only the control gain K_1 takes effect.

Linear quadratic regulator (LQR) technique is applied to design the control gain K_1. Plugging the control law (23) into the model of SEA status (12), the closed-loop error dynamics of SEA status can be derived as

$$\dot{E} = A_e\ E + B_e \left(K_1 E - \hat{d} + d\right) \tag{24}$$

where

$$A_e = \begin{bmatrix} 0 & 1 \\ -\frac{K}{J_s} & -\frac{B_s}{J_s} \end{bmatrix}, \quad B_e = \begin{bmatrix} 0 \\ -\frac{1}{J_s} \end{bmatrix} \tag{25}$$

and d denotes the lumped disturbances from unexpected HEI disturbances and unmodeled system uncertainties, such as friction and imperfect human motion effect compensation. The cost index of the closed-loop system is chosen as

$$J = \int_0^\infty \left(E^T Q E + \rho u^2\right)\ dt \tag{26}$$

where Q is a 2×2 positive definite matrix and ρ is a positive constant. The optimal feedback control gain K_1 to stabilize the closed-loop system and minimize the cost index J can be obtained by solving the Riccati equation

$$A_e^T P_e + P_e A_e - \rho^{-1} P_e B_e B_e^T P_e + Q = 0 \tag{27}$$

and calculated as

$$K_1 = [k_{11} \;\; k_{12}] = -\rho^{-1} B_e^T P_e \tag{28}$$

where P_e is a 2×2 positive definite matrix solved from (27).

Meanwhile, a sliding mode (SM) term is adopted to enhance the torque control robustness to reject disturbances as

$$\hat{d} = \kappa \cdot \operatorname{sgn}\left(E^T P_e B_e\right) \tag{29}$$

where κ is the amplitude coefficient and $\operatorname{sgn}(\cdot)$ refers to the sign function.

The stability of the closed-loop CSEA system in SEA status is analyzed in the following theorem.

Theorem 1: Considering the CSEA system operates in SEA status with dynamics (12) and bounded disturbance $|d| \leq \sigma$, if the unified torque controller (19)–(22) with $P = 1$ is applied with $\kappa > \sigma$, the state E of the closed-loop system (24) will asymptotically converge to zero.

Proof: The proof is given in Appendix A.

When the CSEA system operates in CSA status with $P = 0$, the control law of the unified torque controller (19)–(22) can be rewritten as

$$T_a = T_{LP} + T_H + K_2 E + K T_r. \tag{30}$$

Substituting (30) into the model of CSA status (16), the closed-loop error dynamics of the CSEA system in CSA status can be written as

$$\dot{e} = -\frac{(K + k_{21})}{k_{22}} e - \frac{1}{k_{22}} d. \tag{31}$$

The stability of the closed-loop CSEA system in CSA status is analyzed in the following theorem.

Theorem 2: Considering the CSEA system operates in CSA status with dynamics (16) and bounded disturbance $|d| \leq \sigma$, if the unified torque controller (19)–(22) with $P = 0$ is applied with positive k_{21} and k_{22}, the torque tracking error e of the closed-loop system (31) is ultimately bounded.

Proof: The proof is given in Appendix B.

As the CSEA system in transition status operates with SEA status dynamics, the closed-loop error dynamics of transition status with $0 < P < 1$ can be obtained by substituting the control law (19)–(22) into (12) as

$$\begin{aligned} \dot{E} = & \left(A_e + P B_e K_1 + (1 - P) B_e K_2\right) E \\ & + (P - 1) B_e \left(B_s \dot{T}_r + J_s \ddot{T}_r\right) + B_e \left(d - P \cdot \hat{d}\right). \end{aligned} \tag{32}$$

The stability of the closed-loop CSEA system in transition status is analyzed in the following theorem.

Theorem 3: Considering the CSEA system operates in transition status with dynamics (12) and bounded disturbance $|d| \leq \sigma$, the state E of the closed-loop system (32) is ultimately bounded if the unified torque controller (19)–(22) with $0 \leq P < 1$ is applied with a matrix Q' satisfying

$$Q' = K_2^T B_e^T P_e + P_e B_e K_2 + 2\rho^{-1} P_e B_e B_e^T P_e \preccurlyeq 0. \tag{33}$$

Proof: Consider Lyapunov function candidate

$$V_{Te} = E^T P_e E. \tag{34}$$

Based on the closed-loop dynamics (32), the time derivative of (34) can be derived as

$$\begin{aligned} \dot{V}_{Te} = & E^T \left[\left(A_e + B_e K_1\right)^T P_e + P_e \left(A_e + B_e K_1\right)\right] E \\ & + (1 - P) E^T \left[\left(K_2 - K_1\right)^T B_e^T P_e + P_e B_e \left(K_2 - K_1\right)\right] E \\ & + 2 E^T P_e B_e \left[(P - 1)\left(B_s \dot{T}_r + J_s \ddot{T}_r\right) + \left(d - P \cdot \hat{d}\right)\right]. \end{aligned} \tag{35}$$

Substituting (27), (28), and the definition of Q' in (33) into (35), it follows that

$$\begin{aligned} \dot{V}_{Te} = & -E^T \left(Q + \rho^{-1} P_e B_e B_e^T P_e\right) E + (1 - P) E^T Q' E \\ & + 2 E^T P_e B_e \left[(P - 1)\left(B_s \dot{T}_r + J_s \ddot{T}_r\right) + \left(d - P \cdot \hat{d}\right)\right]. \end{aligned} \tag{36}$$

Note that $Q \succ 0$, $\rho > 0$, $0 \leq P < 1$, $|d| \leq \sigma$, and $\kappa > \sigma > 0$ for $\hat{d}$ with definition of (29). If the inequality of (33) is satisfied, then

$$\begin{aligned} \dot{V}_{Te} \leq & -\lambda_{\min}\left(Q + \rho^{-1} P_e B_e B_e^T P_e\right) \cdot \|E\|^2 \\ & - (1 - P) \cdot \lambda_{\min}\left(-Q'\right) \cdot \|E\|^2 \\ & + 2\|E\| \cdot \|P_e B_e\| \cdot \left[(P - 1) \cdot \left|B_s \dot{T}_r + J_s \ddot{T}_r\right| + |d|\right] \\ & - 2P \cdot \kappa \cdot \left|E^T P_e B_e\right| \\ \leq & -\lambda_{\min}\left(Q + \rho^{-1} P_e B_e B_e^T P_e\right) \cdot \|E\|^2 \\ & + 2\|E\| \cdot \|P_e B_e\| \cdot \left(\left|B_s \dot{T}_r + J_s \ddot{T}_r\right| + \sigma\right) \end{aligned} \tag{37}$$

where $\lambda_{\min}(\cdot)$ denotes the minimum eigenvalue of the corresponding matrix, and $\|\cdot\|$ denotes the Euclidean norm of vectors. According to (37), $\dot{V}_{Te} < 0$ as long as

$$\|E\| > \frac{2\|P_e B_e\| \cdot \left(\left|B_s \dot{T}_r + J_s \ddot{T}_r\right| + \sigma\right)}{\lambda_{\min}\left(Q + \rho^{-1} P_e B_e B_e^T P_e\right)}. \tag{38}$$

Therefore, it can be concluded that state E is ultimately bounded, completing the proof. ■

Remark 3: Theorem 3 shows that even the CSEA system practically operates with SEA status dynamics under control of the unified torque controller with an inaccurate indication from the status indicator P, an ultimately bounded error state E can be ensured. Therefore, for practical implementation, the transition torque T_t for the updating law (17) of the status indicator P is expected to be set slightly smaller than the critical torque T_c $(k \cdot \theta_c)$. As a result, the transition status is guaranteed with the dynamics of SEA status to ensure that the unified torque controller can stably achieve a continuous torque control of the CSEA system when operating with status transition between SEA status and CSA status.

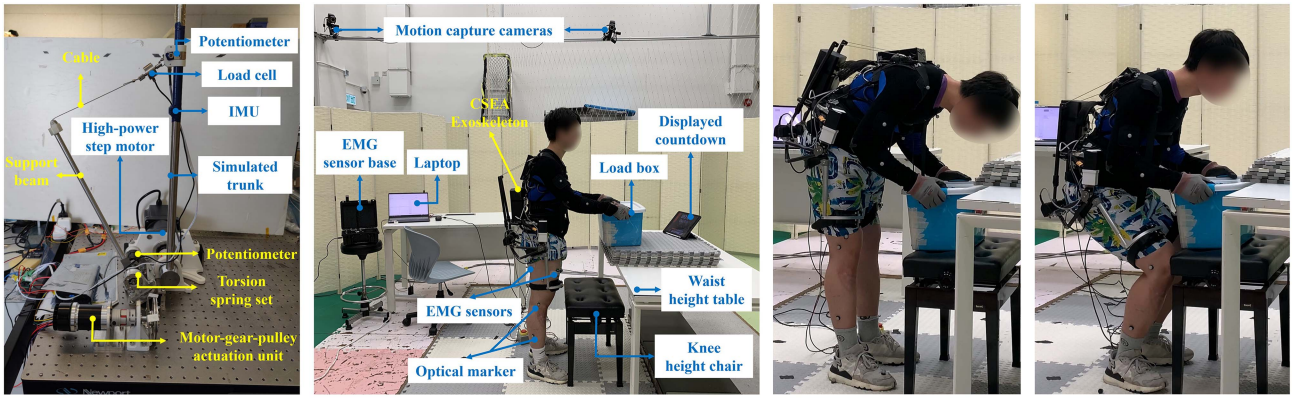

Fig. 10. Experimental setup. (a) Test bench for setup duplication of the CSEA system equipped by the CSEA exoskeleton. (b) CSEA exoskeleton equipped with two CSEA systems. (a) TFE motion in stoop posture and (d) TFE motion in squat posture.

V. Experiments

A. Experimental Setup

To evaluate the performance of the CSEA system and the unified torque controller, bench tests were carried out. Moreover, the closed-loop CSEA system was implemented on the CSEA exoskeleton for human tests to validate its effectiveness for back-support exoskeleton application. The experimental set up of the test bench and the CSEA exoskeleton are shown in Fig. 10.

The specifications of the CSEA system equipped by the CSEA exoskeleton are listed in Table II. The initial angle θ_0 can be adjusted through modifying the support beam tilted angle. A test bench is constructed to duplicate the setup of one CSEA system equipped by the CSEA exoskeleton, as shown in Fig. 10(a). A straight pole is connected to a high-power step motor to simulate the human trunk. The length of the simulated trunk is adjusted to 0.52 m as the measured trunk length of one subject attending the human tests.

The control of the CSEA systems mounted on the test bench and the CSEA exoskeleton prototype shares the same hardware arrangements. A potentiometer (WKA-D22-B, MIRAN, China) and a load cell (JLBM-1, JNSENSOR, China) are applied to measure torsion spring deflection and cable force, respectively. An inertial measurement unit (IMU) (MPU9250, InvenSense, USA) is utilized to measure human trunk kinematic signals, including the trunk flexion angle and angular velocity. The trunk flexion angular acceleration is obtained by differentiating the angular velocity and filtered with a low-pass filter (5 Hz cutoff). A customized microcontroller unit-based (STM32F103CBT6, STMicroelectronics, Switzerland) board is used to implement the unified torque controller to generate control input for actuation unit control via a motor driver, as listed in Table II, and to acquire sensor feedbacks at a frequency of 400 Hz, except for IMU feedback at 200 Hz. Meanwhile, sensor feedback and system states of interest are sent to a laptop for storage at 200 Hz. The frequency setup is unchanged for all the tests unless otherwise stated. For all the tests, the steep level coefficient λ for updating law (17) of P is set as 0.7.

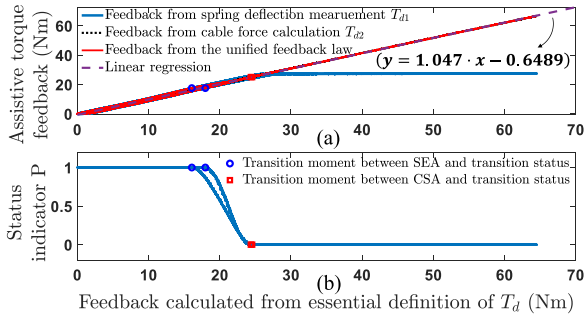

Fig. 11. Assistive torque feedback validation result. (a) Variation of the torque feedback from the unified feedback law with the feedback directly calculated based on definition (1) of T_d and the linear regression conducted for the relationship between the two feedbacks. (b) Status indicator P.

B. System Model Identification

System identification and closed-loop control of the CSEA system require accurate feedback of the delivered assistive torque to ensure that the controlled physical quantity is identical to the targeted object. To validate the accuracy of the assistive torque feedback, the feedback from the unified feedback law (18) was compared with the feedback calculated via the essential definition (1). For calculation via (1), a potentiometer was installed at the cable-simulated trunk connection point, as shown in Fig. 10(a), to measure the intersection angle α_1. The initial angle θ_0 was set as 85°. The deflection constraint was set at 52.5° to allow a wide kinematics variation. For updating of P, T_t was set as 25 N·m, smaller than the critical torque T_c (27.3 N·m). During the test, the simulated trunk was fixed and the motor was rotated to slowly pull the cable. The result is plotted in Fig. 11.

Following the unified feedback law, the toque feedback equals T_{d1} in SEA status with $P = 1$ while equals T_{d2} in CSA status with $P = 0$. As shown in Fig. 11(a), T_{d1} and T_{d2} vary with a close value in SEA status and transition status despite certain hysteresis caused by the backlash and frictions. As a result, the unified torque feedback consistently varies during the transition status, as shown in Fig. 11(a), as well as the status indicator P shown in Fig. 11(b). To evaluate the accuracy of the unified

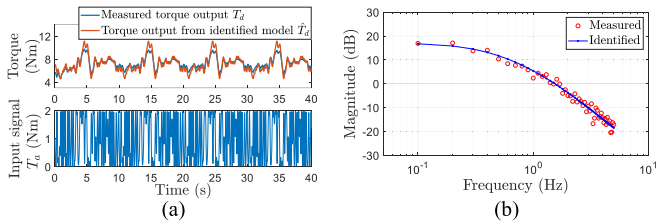

Fig. 12. Measured system responses compared to the identified model responses. (a) Time domain response. (b) Frequency domain response.

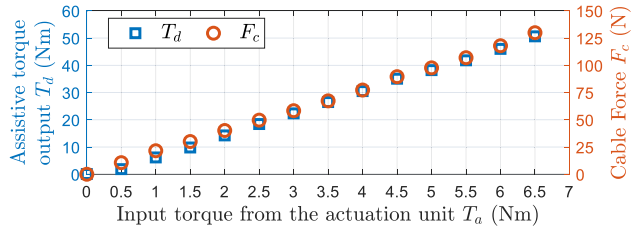

Fig. 13. Assistive torque output range characterization result.

torque feedback, a linear regression is calculated between it and the torque feedback calculated from definition (1). The result presents a linear curve with slope close to 1 and a small offset of -0.6485, indicating accurate feedback for the actual delivered assistive torque. As the feedback components T_{d1} and T_{d2} for unified feedback law are defined based on the system kinematics analysis, the result implies that the system geometry in Fig. 2 can precisely describe the actual CSEA system kinematics.

Based on the verified feedback, the CSEA system model was identified on the test bench to validate the effectiveness of the established model for actual dynamics description and to acquire model parameters for torque controller design. A bias chest-optimized multisine signal with constant power spectral density between 0.1 and 5 Hz, peak value of 2 N·m, and mean value of 1 N·m was generated as the input torque T_a to the CSEA system [62] shown as the bottom plot of Fig. 12(a).

During the identification process, the input torque T_a was updated at 200 Hz and the torque feedback T_d was synchronously collected. The other experimental setups kept unchanged. The SEA status model was identified using System Identification Toolbox [63] in MATLAB (R2021a, The Mathworks, USA) with the input torque signal and torque feedback, and it is given by

$$0.0083\ddot{T}_d + 0.0801\dot{T}_d + 0.1395T_d = T_a + 2.3867\dot{\alpha} + 0.2461\ddot{\alpha}. \tag{39}$$

The result shows that although the amplification coefficient K_s is nonlinear as expressed in (13), it is identified as a constant value of 0.1395. It is close to the theoretical mean value of the nonlinearly varying K_s, which is calculated as 0.1369 based on (5) and (13) with only 1.9% deviation. It again implies high accuracy of the kinematic model of the CSEA system in Fig. 2. As shown in Fig. 12, both overall time domain response and frequency response of the identified model are close to the measured results. To quantify the fitting effect of the identified model, a variance-account-for factor can be calculated as 85.53% following the definition in [61]. The results indicate that although the established model cannot perfectly fit the actual behavior, it is able to describe the major dynamics of the CSEA system in SEA status.

Since CSA status shares same actuation unit and cable transmission with SEA status, for CSA status model (16), K_s follows same definition for SEA status as expressed in (13) and the other coefficients keep identical to the value of SEA status in (39). Hence, the CSA status model coefficients were determined as the same value of SEA status.

C. Bench Tests

To evaluate performance of the closed-loop CSEA system with the unified torque controller and guarantee a safe and effective CSEA system operation for human tests, bench tests were first conducted for system characterization and torque tracking control. A variance-account-for factor was adopted to quantify the torque output fidelity which is defined as [61]

$$\text{fidelity} = \left(1 - \frac{\text{var}\,(Y_d - Y_r)}{\text{var}\,(Y_d)}\right) \cdot 100\% \tag{40}$$

where Y_d is the vector of measured torque output feedback and Y_r is the vector of the sampled sinusoidal or pseudosinusoidal torque command. A fidelity of 100% indicates a torque output without distortion compared to the command.

The parameters of the unified torque controller were determined based on the identified CSEA system models. The identified amplification coefficient of 0.1395 was used as K for the linearization term (20). The index coefficients Q and ρ for (26) were set as diag{1, 0.04} and 1, respectively. As a result, the control gain vector K_1 was calculated as [0.8702, 0.1665] based on the LQR approach. The control gain vector K_2 was finely designed as [1, 0.1913] to satisfy condition (33) for a stable torque control. The deflection constraint was set at 38°, resulting in a critical torque of 19.76 N·m. Accordingly, T_t for the updating of P was set as a smaller value of 18.2 N·m. The coefficient κ of the disturbance rejection term (29) was tuned as 1. The setup was kept unchanged throughout the tests unless otherwise stated. An initialization process was programmed to rotate the motor for a slightly taut cable to make the initial θ_b equal to θ_0. With this initialization, the cable slack was eliminated to avoid instability from zero torque command tracking due to cable slack. Accordingly, the initial positions of the support beam and simulated trunk were zero-reference point of their angular position correspondingly.

1) CSEA System Characterization: To characterize the assistive torque output range, the actuation unit output torque T_a was commanded from 0 with step increment of 0.5 N·m until the output exceeds 50 N·m to meet the requirement listed in Table I. The initial angle θ_0 was set as 85° and the simulated trunk was fixed. As shown in Fig. 13. The CSEA system outputs an assistive torque of 50.63 N·m with a T_a of 6.5 N·m. The result also shows that the cable force for the torque output is 130 N, resulting in a force of 88.7 N parallel to the trunk with the α_1 of 47°. Thus, both the overall force and parallel force are much lower than the comfort limit of 310.5 N and the required 555.6 N for the conventional cable-driven actuation systems.

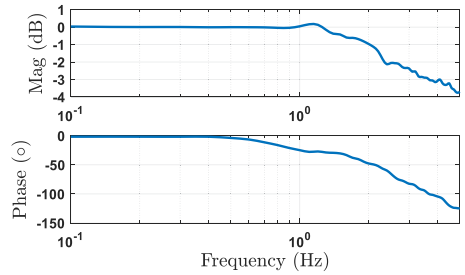

Fig. 14. Bode plot of the closed-loop CSEA system in SEA status with the unified torque controller.

As the torque bandwidth of SEA status is limited by the intrinsic compliance compared with the CSA status, the torque bandwidth of the closed-loop CSEA system was characterized as that of the SEA status. A bias chest-optimized multisine signal with constant power spectral density between 0.1 and 5 Hz, peak value of 20 N·m, and mean value of 15 N·m was generated as input signal T_r. The initial angle θ_0 was set as 85° and the simulated trunk was fixed. The deflection constraint was set at 52.5° to ensure the CSEA system operate in SEA status. Accordingly, T_t for updating law (17) of P was set as 25 N·m. During the test, T_r was updated at the frequency of 200 Hz and the torque feedback of T_d was synchronously collected. The transfer function of the closed-loop CSEA system was estimated using Welch method, and the validity is guaranteed with coherences larger than 0.9. The Bode plot of the estimation result is shown in Fig. 14. It presents a torque bandwidth of 3.65 Hz where magnitude attenuation reaches to 3 dB. Due to the intrinsic compliance in SEA status, the bandwidth is not broad but exceeds the desired 0.5 Hz to satisfy the requirement as listed in Table I.

The output impedance of the closed-loop CSEA system, which is defined as the transfers from load-side motion states, i.e., TFE motion states, to resultant interaction torque, was characterized. Applying cable transmission, the backdrive torque of the CSEA system is zero in the trunk extension direction, which leads to a loose cable. The interaction torque on the human trunk would also be zero when the wearer moves the body with the θ_b between support beam and human trunk smaller than the initial angle θ_0 with a slack cable. Here, the torque command T_r was specified as 1 N·m to keep the cable slightly taut to enable effective measurement of the interaction torque under load-side motions. The initial angle θ_0 was set as 30°. During the test, the simulated trunk was excited by hand for a pseudosine movement with amplitude of around 5° and frequency about 0.5 Hz. As shown in Fig. 15, the interaction torque varies around the command of 1 N·m with an amplitude of below 0.2 N·m. It indicates that besides a zero output impedance with a slack cable, the closed-loop CSEA system with taut cable also exhibits low output impedance for minor resistance on unresisted human motion.

2) Torque Tracking Control of SEA Status: The torque tracking performance was first evaluated for SEA status. To replicate back-support exoskeleton application scenario, the simulated trunk was controlled to simulate TFE motion. As the TFE motion exhibits an approximate sinusoidal profile [64], the simulated TFE motion was specified as

$$\alpha = \frac{A}{2} + \frac{A}{2} \cdot \sin\left(2\pi f_d \cdot t - \frac{\pi}{2}\right) \tag{41}$$

where A determines the maximum flexion angle and f_d refers to the simulated TFE motion frequency. f_d is set as 0.25 and 0.5 Hz to simulate normal and fast TFE motion, respectively. A is set as 60°. The initial angle θ_0 was set as 30°. The simulated trunk was controlled to rotate for three cycles of the simulated TFE motion during the test. The torque command was generated following an impedance strategy as:

$$T_r = k_p \cdot (\alpha - \alpha_0) \tag{42}$$

where α is flexion angle of the simulated trunk measured by an IMU. k_p was set as 0.2 N·m/° and α_0 was set as 0.

The tracking results are shown in Fig. 16. The root-mean-square (rms) tracking errors under simulated TFE motion at the two frequencies are smaller than 5% of the torque output range with a torque fidelity over 98%, as listed in Table III.

3) Torque Tracking Control With Status Transitions: The torque tracking performance of the closed-loop CSEA system when operating with status transitions was also evaluated. The simulated trunk motion and assistive torque command generation followed identical law as in the tests for SEA status. Considering the critical torque of the CSEA system is 19.76 N·m, k_p was set as 0.5 N·m/° so that the operation status would transition between SEA status and CSA status with a peak torque command of 30 N·m.

The experimental results are shown in Fig. 17. It can be seen from the first-row plots that when the torsion springs can be

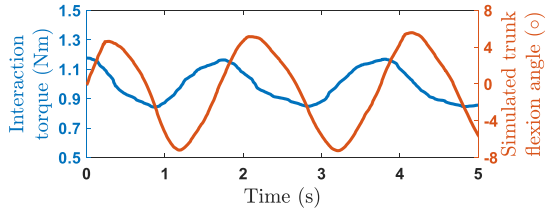

Fig. 15. Interaction torque from the closed-loop CSEA system under a pseudosine movement of the simulated trunk excited by hand. The torque command is set as 1 N·m instead of 0 to keep the cable slightly taut.

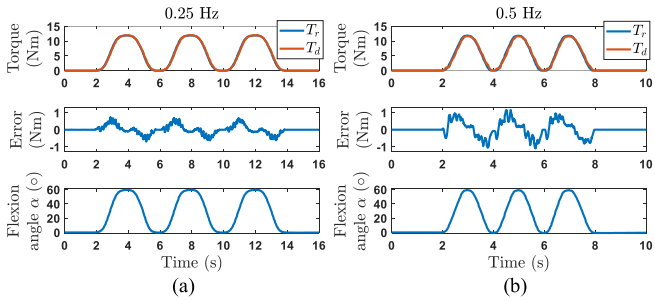

Fig. 16. Torque tracking performance of the closed-loop CSEA system in SEA status with moving simulated trunk for simulated TFE motion at two frequencies. (a) 0.25 Hz. (b) 0.5 Hz.

TABLE III
RMS TRACKING ERROR (UNIT: N·M) AND TORQUE FIDELITY (WITH GRAY BASE COLOR) OF TORQUE TRACKING CONTROL TESTS WITHIN BENCH TESTS

CSEA System Operation Status	Frequency of the simulated TFE	
	0.25 Hz	0.5 Hz
SEA Status	0.2790	0.5832
	99.65%	98.36%
Transition between SEA status and CSA status	0.9093	1.4722
	99.13%	98.02%

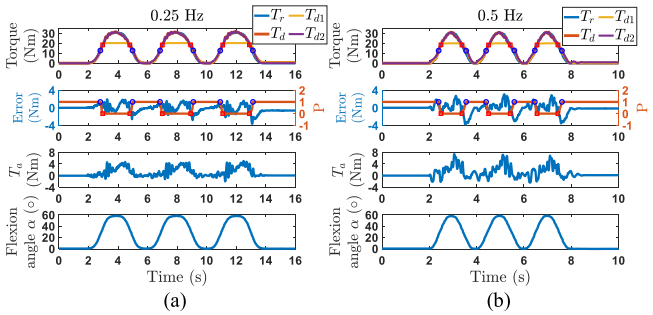

Fig. 17. Torque tracking performance of the closed-loop CSEA system operating with status transition between SEA status and CSA status with moving simulated trunk for simulated TFE motion at two frequencies. (a) 0.25 Hz. (b) 0.5 Hz. The blue circles and the red squares refer to the transition moments between SEA status and transition status and between CSA status and transition status, respectively.

freely deflected, the torque feedback T_{d1} from torsion spring deflection measurement varies close to the feedback T_{d2} from cable force calculation. Smooth and consistent assistive torque feedback and status indicator variation are thus guaranteed as shown in the first-row and second-row plots of Fig. 17. This is consistent with the torque feedback validation result in Fig. 11, indicating the precise kinematics analysis in Fig. 2. It also verified that the inertia omission in (9) for model establishment of SEA status has a negligible effect on the accuracy of the dynamic assistive torque feedback.

The tracking results in the first-row plots demonstrate that the CSEA system effectively outputs an assistive torque over 30 N·m, which exceeds the maximum torque output 28.37 N·m of SEA status limited by torsion springs with a maximum safe deflection of 54.55°. The control input T_a from the unified torque controller is illustrated in the third-row plots, presenting a continuous variation despite the discontinuous CSEA system dynamics during status transitions. With the continuous control input, a smooth torque output is attained in SEA and transition status, but the output shows certain small oscillations in CSA status. Despite this, an overall consistent and accurate tracking effect is achieved as shown in the first-row plots. As listed in Table III, the rms tracking error is lower than 5% of the torque output range while a torque fidelity over 98% is achieved for the tracking under simulated TFE at the two frequencies. The results demonstrated that the CSEA system operating with multiple statuses can overcome the output limitation of SEA status for a large assistive torque output capability. Meanwhile, the results

TABLE IV
RMS TRACKING ERROR (UNIT: N·M) AND TORQUE FIDELITY (WITH GRAY BASE COLOR) OF TORQUE TRACKING CONTROL TESTS WITHIN HUMAN TESTS

CSEA System Operation Status	The CSEA system on the exoskeleton		
	Left	Right	Overall
SEA Status	0.5015	0.5415	1.0213
	99.33%	99.30%	99.26%
Transition between SEA status and CSA status	0.8275	0.9956	1.7052
	99.23%	99.28%	99.31%

indicate that with the unified torque controller, the CSEA system can stably transition between SEA status and CSA status to generate desired assistive torque consistently and accurately.

D. Human Tests

Human tests were carried out based on the CSEA exoskeleton, as shown in Fig. 10(b), to validate the effectiveness of the closed-loop CSEA system for practical back-support exoskeleton actuation. Five male subjects [mean ± standard deviation (SD): age, 27.6 ± 3.1 years; mass, 71.4 ± 5.3 kg; height, 174.4 ± 8.6 cm] with no low back injury in past six months were recruited for the test. In the human tests, the same initialization process for bench tests was programmed to rotate the motor for a slightly taut cable to make the initial equal θ_b to θ_0.

1) Torque Tracking Control Tests: During the tracking control tests, one subject wore the CSEA exoskeleton to perform TFE motion in a stoop posture with a 5-kg load in hand for three cycles at preferred speed. The performance index coefficient Q and ρ were finely tuned as diag{1, 0.015} and 1, respectively, through pilot experiments. The feedback control gain vector K_1 was calculated as [0.8702, 0.1091] based on the LQR approach. The feedback control gain vector K_2 was designed as [1, 0.1254] to satisfy condition (33). The coefficient κ of the disturbance rejection term (29) was set as 1. The hardware setup was identical for the two CSEA systems and controller parameters were kept unchanged throughout the tracking control tests.

a) Torque tracking control of SEA status: First, the torque tracking performance of the closed-loop CSEA systems in SEA status was evaluated. The command for each CSEA system was generated based on strategy (42) with k_p and α_0 set as 0.2 and 0, respectively. To ensure the CSEA system operate in SEA status, the deflection constraint was set at an angle of 50° with T_t accordingly set as 25.5 N·m for updating of P. The initial angle θ_0 was set as 10°.

The experimental results are shown in Fig. 18. Both the left and right CSEA systems present an accurate tracking, showing an rms tracking error of 1.0213 N·m for the overall assistive toque tracking, as listed in Table IV, which is only 3.02% of the peak toque command of 33.84 N·m. Meanwhile, a torque fidelity over 99% is achieved for the torque output of two CSEA systems, as well as the overall torque output.

b) Torque tracking control with status transitions: In this experiment, the deflection constraint was set at 37° for a critical torque value of 19.24 N·m and T_t was set as 17.68 N·m for

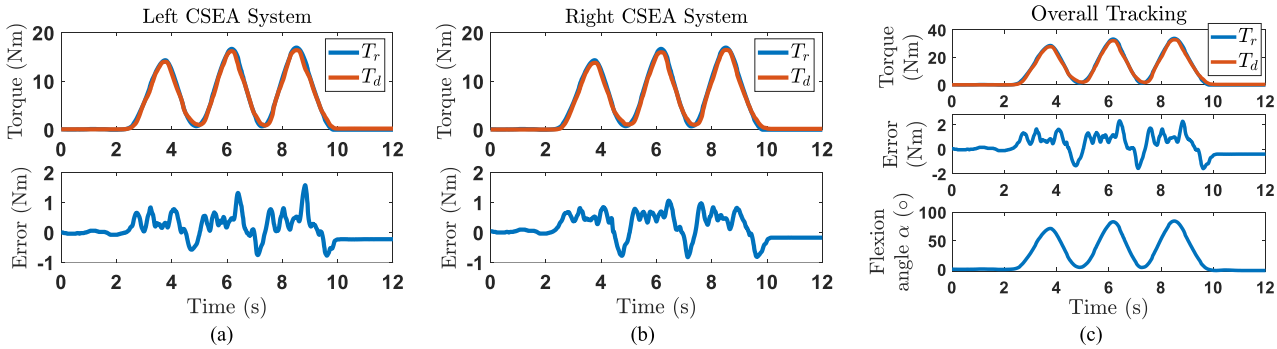

Fig. 18. Assistive torque tracking performance of the closed-loop CSEA systems in SEA status during back-support exoskeleton implementation. (a) Left CSEA system. (b) Right CSEA system. (c) Overall tracking performance for back-support exoskeleton operation.

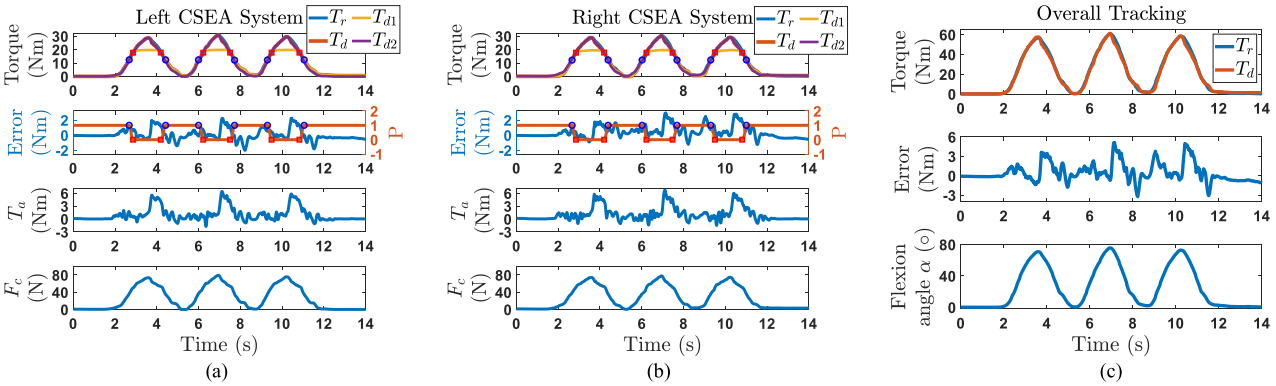

Fig. 19. Assistive torque tracking performance of the closed-loop CSEA system operating with status transition between SEA status and CSA status during back-support exoskeleton implementation. (a) Left CSEA system. (b) Right CSEA system. (c) Overall tracking performance for back-support exoskeleton operation. The blue circles and the red squares refer to transition moments between SEA and transition status and between CSA and transition status, respectively.

updating of P. The initial angle θ_0 was adjusted to 15°. To lead to status transition, the command for each CSEA system was generated following (42) with k_p and α_0 specified as 0.4 and 0, respectively.

The experimental results are presented in Fig. 19. Similar to the results in Fig. 17, with a close T_{d1} and T_{d2} in SEA status and transition status, smooth and consistent torque feedback and status indicator P are guaranteed during the tracking, as shown in first-row and second-row plots of Fig. 19(a) and (b). It indicates that the system geometry shown in Fig. 2 can accurately describe the kinematics of the CSEA system during back-support exoskeleton implementation. Fig. 19(a) and (b) shows that a maximum torque over 30 N·m is generated from each CSEA system in CSA status, resulting in a peak exoskeleton assistance output over 60 N·m. Considering that the maximum torque output of SEA status is 28.37 N·m, the CSEA system successfully overcomes the torque output limitation of SEA status. The cable force is shown in the fourth-row plots of Fig. 19(a) and (b), which is below 80 N for the torque output over 30 N·m, verifying the efficient assistive torque output capability of the CSEA system.

Although there are operation status transitions during the tracking, a continuous control input T_a is generated from the unified torque controller, as shown in the third-row plots of Fig. 19(a) and (b). With this control input, a consistent and accurate torque tracking is achieved despite the discontinuous CSEA system dynamics during status transitions as verified in the first-row plots of Fig. 19(a) and (b). Moreover, it can be observed that with inherent compliance from human tissues and a smooth TFE motion, as shown in Fig. 19(c), the torque output in CSA status is as smooth as that in SEA status and transition status, eliminating the oscillations appearing in the bench test shown in Fig. 17. As listed in Table IV, both left and right CSEA systems achieved an accurate tracking, leading to an rms tracking error of 1.7052 N·m for the overall toque tracking, which is 2.82% of the peak toque command of 60.52 N·m. Meanwhile, the tracking results present a fidelity over 99% for the torque output of each CSEA system, as well as for the overall torque output. The results validate the efficacy of the closed-loop CSEA system for back-support exoskeleton actuation to stably, consistently, and accurately generate desired torque for TFE motion assistance.

2) Trunk RoM Test: This RoM test was carried out to evaluate the effect of the CSEA exoskeleton on the wearer's trunk RoM. The five subjects were instructed to bend the trunk in three directions for flexion, lateral bending, and axial rotation. The motions were required to be performed for three repetitions with or without wearing the CSEA exoskeleton, respectively.

TABLE V
TRUNK RANGE OF MOTION

	Flexion	Lateral Bending	Axial Rotation
Without Exoskeleton	124.0° ± 2.5°	53.1° ± 7.3°	85.5° ± 2.5°
With Exoskeleton	119.1° ± 5.1°	50.6° ± 7.1°	85.2° ± 2.7°

When wearing the exoskeleton, the two CSEA systems were controlled to maintain a tensioned cable with a certain force. The trunk kinematics were recorded by a motion capture system (VICON, Oxford Metrics, U.K.) at 100 Hz and the peak trunk bending angles in three directions were extracted using custom MATLAB routines. The resulting trunk RoMs are listed in Table V, demonstrating a reduction of 4.0%, 4.7%, and 0.6% in the three directions while wearing the CSEA exoskeleton compared with no exoskeleton condition.

3) Preliminary Electromyography (EMG) Test: To evaluate efficacy of the CSEA exoskeleton assistance, the activation of relevant muscles during TFE motion was investigated. The five subjects attended the EMG test in the following day after completing the RoM test. In the EMG test, each subject was asked to perform ten cycles of TFE motion with two different postures [stoop and squat posture as shown in Fig. 10(c) and (d)] and exoskeleton conditions (with and without wearing the CSEA exoskeleton). During each TFE motion cycle, the subject was required to grasp a 15-kg load from a waist height table, flex the trunk to lower the load to a knee height chair, then grasp the load again and extend the trunk to lift it back to the table. In the test, although the TFE speed was not explicitly controlled, each TFE motion cycle was instructed to be completed within a 6-s countdown. To reduce intervention of muscle fatigue, a 10-s countdown was displayed on a screen to instruct a rest interval between two consecutive TFE motion cycles. The assistive torque command for each exoskeleton equipped CSEA system was generated following (42) with k_p and α_0 setting as 0.2 and 0, respectively. α in (42) was fed with trunk flexion angle and hip joint flexion angle to generate the assistance command for stoop posture and squat posture, respectively. The CSEA system specifications and controller parameters were set identical to the tracking control tests.

During the test, the human kinematics were recorded by the motion capture system for offline segmentation of TFE motion cycle. The EMG signals of five bilateral groups of muscle, which are erector spinae longissimus (ESL), erector spinae iliocostalis (ESI), biceps femoris (BF), rectus femoris (RF) and rectus abdominis (RA), were recorded via wireless EMG sensors (Trigno system, Delsys, USA) at 2000 Hz. The collected EMG signals were demeaned, band-pass filtered (20 to 300 Hz), rectified, and low-pass filtered (3 Hz cutoff). RMS of the EMG signal of each muscle group was calculated and normalized by the maximum processed EMG signal to quantify the muscle activation intensity. The normalized EMG were averaged between the left-hand and right-hand sides, reported as the mean ± standard error of the mean over the results of each subject for the TFE motion cycle under different posture and exoskeleton conditions. As shown in Fig. 20, the results indicate reduction of the back and hip muscle activation intensity while wearing the exoskeleton compared with no exoskeleton condition (for ESL, ESI, BF, and RF, respectively: 27.2%, 27.0%, 14.9%, and 12.8% in stoop posture; 22.7%, 17.5%, 21.5%, and 32.3% in squat posture). The abdominal muscle RA exhibits small activation variations, for a 1.2% increase in stoop posture and a 5.5% decrease in squat posture.

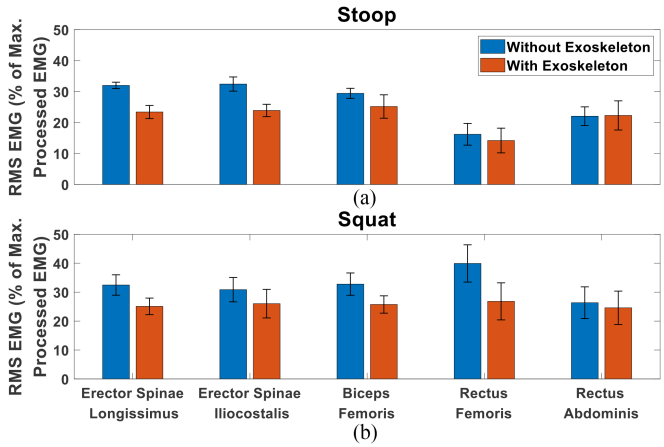

Fig. 20. RMS EMG of relevant muscle groups during TFE motion in (a) stoop posture and (b) squat posture.

VI. DISCUSSION

A. Advantages of the CSEA System

The unique design of the CSEA system enables it to achieve sufficient capability to meet our targets for the back-support exoskeleton actuation system, as concluded in Table I. Section II-D showed the CSEA system can generate a 75 N·m assistive torque under a TFE velocity of 2.42 rad/s. The system characterization tests showed the capability of the CSEA system to efficiently generate an assistive torque above the required 50 N·m with a cable force below half of the comfort limit. The tests also demonstrated a closed-loop CSEA system performance with a torque bandwidth above 7 times of the desired 0.5 Hz and a small output impedance for 0.2 N·m resistive torque with a taut cable. Moreover, the human tests demonstrated that, equipped with CSEA system, the CSEA exoskeleton can effectively assist with different TFE motions and allow 3-D trunk movements with the reduction on the trunk RoM below 5.0%, which is less than those reported in similar studies [29], [65], [66].

Comparisons of the CSEA system with rigid actuation systems and conventional cable-driven actuation systems are presented in Fig. 21. To provide a general quantitative characterization for capability of the actuation system to allow an unrestricted trunk motion, an indicator called actuation flexibility is defined as the number of DoFs of the trunk that the exoskeleton powered by the actuation system can accommodate and assist. Existing back-support exoskeletons powered by rigid actuation systems are typically equipped with two actuators to only accommodate and assist with trunk motion in sagittal plane. Applied with four motors, the exoskeleton with rigid actuation systems in [13] extended the ability to provide assistance in

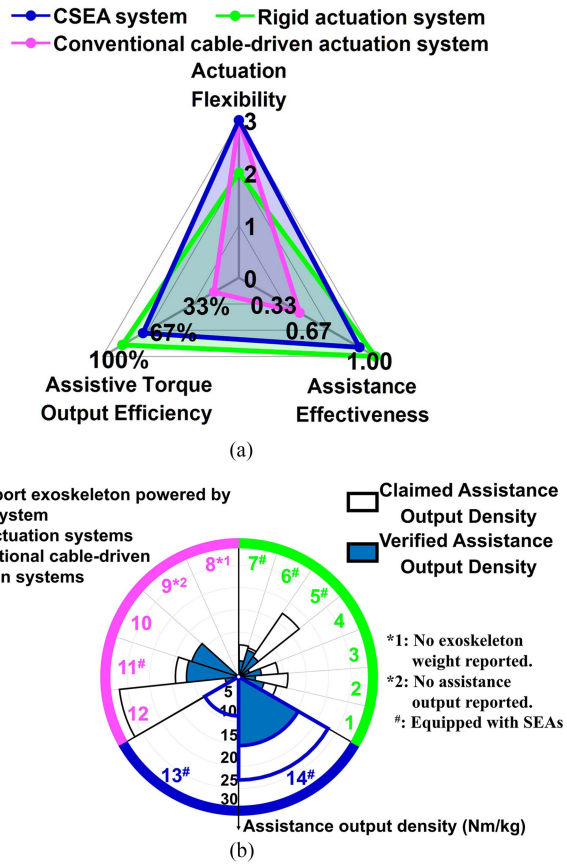

Fig. 21. Comparison of the CSEA system with other back-support exoskeleton actuation systems. (a) Spider diagram for actuation characteristics comparison of the CSEA system with the rigid actuation system and conventional cable-driven actuation system. (b) Assistance output density of the CSEA exoskeleton and existing back-support exoskeletons by other actuation systems. The normalized claimed maximum assistive torque outputs are illustrated with no base color. The normalized verified assistive torque outputs refer to the torque output reported with experimental data and are covered with blue base color. 1-ExoBack (8.4 kg) [6], [67]; 2-Cray X (11 kg) [7], [67]; 3-XoTrunk (8 kg) [8], [68]; 4-APO (8 kg) [9], [58]; 5-H-WEXv2 (5.5 kg) [11]; 6-A lifting assist device (4.4 kg excluding batteries) [12]; 7-A lower-back robotic exoskeleton (11.2 kg) [13]; 8-continumm soft exoskeleton [26]; 9-A soft power suit (2.4 kg) [27]; 10-A back exosuit (2.7 kg) [28]; 11-SHAE (6.2 kg) [29]; 12-ABX (6.4 kg) [30]; 13-CSEA exoskeleton with only SEA status (6.5 kg); 14-CSEA exoskeleton with multiple operation statuses (6.5 kg).

frontal plane besides in sagittal plane. Accordingly, the actuation flexibility of the rigid actuation system is scored as 2. In [28], a back-support exoskeleton powered by conventional cable-driven actuation systems presented the ability to generate 3-DoF torque for asymmetric lifting assistance. Here, the CSEA system can deliver assistive force on both side of the wearer's shoulder under 3-D trunk motion as verified in the RoM test, implying the capability of generating assistive torque over three axes of the lumbosacral joint. Hence, the conventional cable-driven actuation system and the CSEA system present a superior actuation flexibility with a score of 3 compared with rigid actuation systems as depicted in Fig. 21(a).

An indicator named assistive torque output efficiency is calculated by normalizing the assistive force moment arm within the actuation system to a trunk length of 0.492 m. A higher value of the indicator signifies higher assistive torque output efficiency with lower demand of cable force. Accordingly, as analyzed in Section II-C, the CSEA system can obtain a 3.8 times higher efficiency (70.3%) compared to that of conventional cable-driven actuation systems (18.3%) with a moment arm around 0.09 m [26], [27], [28], [29], [30], which is slightly smaller than the rigid actuation system (85.4%) with a moment arm around 0.42 m [11], [12], [15], as depicted in Fig. 21(a). The results in Fig. 13 verified the high efficiency of the CSEA system to output a 50 N·m assistive torque with a cable force of 130 N below the comfort limit of 310.5 N. In comparison, a cable force of 555.6 N, which exceeds the limit, is required by the conventional ones. This enables the CSEA system to provide sufficient TFE assistance without rising risk of structure fracture or threatening the safety and comfort of HEI by reducing the force transmitted within the actuation system and exerting on human trunk.

With the high assistive torque output efficiency and a bias cable force output, as shown in Fig. 2, the CSEA system can greatly reduce the force applied parallel to the trunk compared with the conventional cable-driven actuation system, when subjected to an identical assistive torque output. Hence, from biomechanical perspective, the CSEA system is expected to achieve a higher lumbar compression alleviation with less lumbar compression resulted from the parallel force [15], [31]. An indicator, named as assistance effectiveness, is defined to indicate expected lumbar compression alleviation effect. It is calculated by normalizing the difference between the estimated spinae muscle forces for unit biological TFE moment and the parallel force under unit assistive torque output to the spinae muscle forces. With a trunk length of 0.492 m, for CSEA system with specifications in Table II, the averaged parallel force F_c' under unit assistive torque output shown in Fig. 2 is computed based on (5) as 2.07 N. For the conventional cable-driven actuation system with moment arm of 0.09 m, the parallel force equals to the overall required cable force of 11.1 N. The moment arm of spinae muscle force for biological TFE moment generation is assumed as 0.05 m [69] so that a 20-N spinae muscle force is needed for unit TFE moment output. It can then be calculated that the assistance effectiveness of the CSEA system (0.897) is slightly lower than the rigid actuation systems (1.0) with no parallel force component, but largely exceeds the conventional cable-driven actuation systems (0.444), as depicted in Fig. 21(a). It indicates that besides a safe and comfortable HEI, under identical assistive torque output, the CSEA system is expected to achieve a higher lumbar compression reduction compared with the conventional cable-driven actuation system from the biomechanical perspective.

Fig. 21(b) shows the comparison of the assistance output density, which is calculated as the maximum assistive torque output above the exoskeleton weight, between the CSEA exoskeleton powered by two CSEA systems and back-support exoskeletons powered by other types of actuation systems. With the superior actuation characteristics illustrated in Fig. 21(a), the CSEA system enables a verified assistance output density of 15.38 N·m/kg for the CSEA exoskeleton weighted 6.5 kg. As shown in Fig. 21(b), it is higher than that of other cable-driven exoskeletons, which often limit practical assistive torque output

to a lower value than claimed output to avoid user discomfort from overlarge cable force as in [30], or designed with a low targeted maximum assistance output as in [28], or lack reporting of assistance output as in [27]. Moreover, as analyzed in Section II-D, the CSEA exoskeleton can operate with multiple statuses to overcome the torque output limitation of SEA status for a maximum assistive torque output of 150 N·m. It thus presents an assistance output density of 23.08 N·m/kg, which is higher than the CSEA exoskeleton with only SEA status and the SEA-actuated exoskeletons that reported output limitations from SEA [11], [12], [29], as indicated in Fig. 21(b). It can also be seen that with multiple operation statuses, the CSEA exoskeleton achieves an assistance output density exceeding other compared back-support exoskeletons. With the high assistance output density, the CSEA exoskeleton also serves as a versatile experimental platform with a light weight and ample output capability to allow for exploration of a board spectrum of assistance profiles.

B. Performance of the Unified Torque Controller

The unified torque controller is proposed as a generic solution to guarantee a stable, continuous, and accurate torque control for the actuation system like the CSEA system whose operation status can transition between SEA status and CSA status. The torque tracking control results in Figs. 16–19 verified the desired tracking performance, regardless of whether the CSEA system operating in sole SEA status or with status transitions, with a torque fidelity above 99% and rms tracking error below 4% of the torque output range on average. Theoretically, the sufficient conditions to guarantee the stability of the closed-loop CSEA system are derived. The stability analysis suggests that as long as the control gain was set satisfying the sufficient condition, the compensation and disturbance rejection term can be extended with other techniques without affecting the stability. It implies the efficacy of the proposed controller to be adapted and extended as a generic frame to stably and robustly ensure a continuous and accuracy control for the class of the actuation system like the CSEA system in different scenarios.

Although an accurate torque tracking with small rms error is achieved, the torque tracking test results showed that there exist relatively large peak tracking errors around the onsets of TFE motion. It can be partially explained by the imperfect human motion effect compensation. As implied in the system identification results in Fig. 12, there are certain difference between identified inertia parameters used for the motion effect compensation term (21) and their actual values. Hence, the compensation term cannot precisely counteract the human motion effect especially at the motion onsets with a high acceleration. Another potential reason is the presence of friction effects. The cable transmission needs to overcome static friction for an initial speed to deliver the desired force at the motion onsets. Moreover, the reversing cable velocity direction during the CSEA system operation can affect the tracking with a changing friction direction. These effects from frictions and imperfect compensation raise the requirement for the controller to improve uncertainty and disturbance rejection ability to further enhance the tracking accuracy.

Also, when an overall consistent tracking was achieved, the torque output in the CSA status showed certain oscillations in bench tests, as shown in first-row plots of Fig. 17. This may be mainly attributed to the shaking of the simulated TFE motion. As shown in fourth-row plots in Fig. 17, the simulated trunk in the test bench, which is driven by a step motor, vibrates especially in the vicinity of the peak flexion angle in the CSA status where a high force is applied, inducing intensive disturbances. The oscillations may be further explained by considering the CSEA system in CSA status, where a stiff interface between actuation unit output and load side reduces the system tolerance for the impact disturbances compared with SEA status with a compliant interface. With a smooth TFE motion and intrinsic compliance from the interaction harness and human tissue, there was no oscillation observed in CSA status during the tracking in human tests, as shown in Fig. 19. Although a good tracking performance is achieved for practical exoskeleton actuation, the bench test results indicate that the realization of a compliant torque control for the CSEA system is important for future controller improvement to robustly guarantee smooth tracking under various conditions.

C. Assistance Effect of the CSEA Exoskeleton

The CSEA exoskeleton is developed to leverage advantages of the CSEA system to assist with TFE motion ergonomically and effectively for the reduction of relevant muscle activity and lumbar compression. The EMG test showed that with the CSEA exoskeleton assistance, the activation intensity of the erector spinae muscle was reduced by 27.1% and 20.1% on average for the TFE motion in stoop posture and squat posture, respectively. The results verified the effectiveness of the CSEA exoskeleton in reducing back muscle activity with a reduction comparable to the average level of other active back-support exoskeletons [70]. Meanwhile, compared to many cable-driven back-support exoskeletons only reporting assistance effect for stoop posture [26], [27], [29], [30], the results demonstrated the versatility of the CSEA exoskeleton to effectively assist with different lifting postures.

In addition to the back muscles, the activation intensity reduction can also be observed for the hip muscles, including the hip flexor RF and hip extensor BF. The EMG test results showed that reduction extents of the hip muscles' activation intensity during TFE motion in squat posture were greater than that in stoop posture. It may be attributed to the higher activation level of the hip muscles than in the stoop posture as the TFE motion in squat posture is primarily governed by the hip joint, whereas flexion of lumbosacral joint is more prominent than hip joint in stoop posture [71]. Regardless, the results demonstrated the efficacy of the CSEA exoskeleton in assisting not only lumbosacral joint motion but also the hip joint motion during TFE for reduced muscle activity.

Moreover, in contrast to some similar studies reporting a large or consistent increase in abdominal muscle activity [12], [30], [72], the EMG test presented small variations of the tested abdominal muscle activity. It implies that the assistance can keep synergistic with the wearers' biological response to reduce the

muscle activity of relevant back and hip muscles without raising antagonistic reactions of the abdominal muscles. This strongly suggests that powered by the CSEA system, the CSEA exoskeleton can effectively assist with TFE motion while maintaining an ergonomic HEI.

D. Limitations

Although the CSEA system successfully powered the CSEA exoskeleton for effective TFE motion assistance, there are still some limitations remain to be overcome to further improve its usability. A primary limitation is the obtrusiveness from the lagging support beam. When the structural specifications of the CSEA system are determined to guarantee a successful system operation with a positive intersection angle between the support beam and human trunk, this angle can lead to a lagging support beam behind the wearer's trunk. As a result, it can result in obtrusiveness and increase the risk of unexpected interaction of between the beam and external environment, posing a potential threat to the HEI safety. In the future, the CSEA system could be enhanced with a motorized stiffness modulation mechanism to automatically adjust the torsion spring set stiffness so that the support beam can well adapt to different assistance profiles with minimized angle relative to the trunk to reduce obtrusiveness. Moreover, an elastic cover can be added to envelop the torsion spring–support beam mechanism to eliminate the safety risk brought by the exposed beam and cable, and to facilitate a more compact CSEA system design. Another limitation is that when it is mentioned various advantages are enabled by the unique design of the CSEA system, some features require more detailed characterization. Specifically, when the capability of the CSEA system to deliver assistive force under 3-D trunk posture has been demonstrated in the RoM test, the CSEA system kinetics with trunk posture outside the sagittal plane could be modeled to specify the output range of the assistance at each DoF of the trunk. In addition, the inference of better lumbar compression alleviation with lower force parallel to trunk compared with conventional cabled-driven actuation systems in Section VI-A was drawn based on intuitive biomechanical considerations. The parallel force effect on the spinal joint load should be further investigated using advanced techniques, such as musculoskeletal modeling or inverse human dynamics modeling.

The performance of the unified torque controller can also be further enhanced by overcoming certain limitations to improve the tracking accuracy and smoothness. When the controller considered compensation of human motion effect, a feedforward model-based friction compensation could be added into the control law to explicitly compensate the friction effects. Although the controller adopts an SM term to reject disturbances, it only takes effect in SEA status. Moreover, its practical effect is limited by the lack of capability to precisely estimate the disturbance and the compromised responsiveness due to replacement of sign function $\mathrm{sgn}(\cdot)$ by saturation function $\mathrm{sat}(\cdot)$ during practical implementation for chattering avoidance. To improve the robustness against disturbances, the controller is expected to attain the ability to actively estimate and continuously compensate disturbances in both SEA status and CSA status as well as the transition status by adopting advanced control methods, such as adaptive control and disturbance observer-based control. On the other hand, the torque output oscillations occurred during the tracking in CSA status imply that the unified torque controller lacks consideration for a compliant torque control to guarantee a smooth tracking under different disturbances. To do so, in the future, the proposed unified controller frame can be extended with compliant control law, such as the proxy-based torque control [49], to not only keep a robust and accurate tracking under normal operation, but also guarantee a compliant control under unexpected disturbances.

When the EMG test results provided evidence supporting the effectiveness of CSEA exoskeleton assistance on reduction of related muscle activity and lumbar compression during TFE motion, there are still some limitations for the test setup. First, thought two different lifting postures were tested, the singular setup of the load weight and trunk flexion range limits the generalization of the results to other scenarios. Second, the small number of the subjects limits the efficacy of the statistical analysis, thereby preventing us from concluding significance of the results. Third, diversity of the subjects is limited. When the target users are workers who regularly engage in MMH work, current recruited subjects consisted solely of research students and research staffs, who may have divergent biological responses to the exoskeleton assistance compared with the workers. In the future, to fully study the exoskeleton assistance effect, tests with more comprehensive setup should be conducted. The tests would involve evaluating biomechanical and physiological response during TFE motion with various load weights, encompassing different practical MMH work conditions. Furthermore, to better ensure the validity of the results, a sufficient number of actual workers would be recruited for the future test.

VII. Conclusion

This article introduced a novel CSEA system and its torque controller to realize a flexible and portable back-support exoskeleton design with capability to ergonomically, efficiently, and accurately generate desired sufficient assistance.

The effectiveness of the CSEA system and the proposed unified torque controller is experimentally validated. System characterization results in bench test validated the low mechanical impedance, sufficient torque bandwidth, as well as sufficient and efficient torque output capability of the closed-loop CSEA system to satisfy our targets for back-support exoskeleton actuation system design. The torque tracking control tests in both bench test and human test validated that the closed-loop CSEA system is able to stably, consistently, and accurately generate desired assistive torque despite the discontinuous system dynamics during operation status transition. Meanwhile, the human test verified the effective implementation of the closed-loop CSEA system on a flexible and portable back-support exoskeleton. The RoM test demonstrated that the CSEA exoskeleton equipped with the CSEA system can ergonomically adapt to different trunk postures with minor limitation on the natural RoM. Moreover, the EMG test presented effective muscle activity reduction for the relevant back and hip muscles during

the TFE motions with the assistance from the CSEA exoskeleton. The results indicate that the proposed closed-loop CSEA system can not only satisfy our target requirements, but also present advantages in realizing a flexible, efficient, and powerful back-support exoskeleton actuation compared with existing counterparts. It thus provides a promising method to develop a back-support exoskeleton to maximize biological benefits for TFE assistance with an efficient and sufficient assistance output capability while minimizing restrictions on other natural motions with a flexible and ergonomic structure.

APPENDIX

A. Stability of the Closed-Loop CSEA System in SEA Status

Consider Lyapunov function candidate

$$V_{Se} = E^T\ P_e E. \tag{43}$$

Based on (23), (24), (27), and (29), the time derivation of (43) can be derived as

$$\begin{aligned}\dot{V}_{Se} = &E^T\ \left(A_e^T P_e + P_e A_e - 2\rho^{-1} P_e B_e B_e^T P_e\right) E \\ &+ 2E^T P_e B_e \left(-\kappa \cdot \operatorname{sgn}\left(E^T P_e B_e\right) + d\right) \\ \leq &-E^T \left(Q + \rho^{-1} P_e B_e B_e^T P_e\right) E \\ &- 2\left|E^T P_e B_e\right| \cdot \kappa + 2\left|E^T P_e B_e\right| \cdot \sigma \\ = &-E^T \left(Q+\rho^{-1} P_e B_e B_e^T P_e\right) E - 2\left|E^T P_e B_e\right| (\kappa-\sigma).\end{aligned} \tag{44}$$

According to (44), since $\kappa > \sigma$, $\dot{V}_{Se} < 0$ is guaranteed with the positive definite matrix Q and the positive constant ρ. Therefore, the state E will asymptotically converge to zero. ■

B. Stability of the Closed-Loop CSEA System in CSA Status

Consider Lyapunov function candidate

$$V_{De} = \frac{1}{2} e^2. \tag{45}$$

Based on (31), the time derivation of (45) is derived as

$$\begin{aligned}\dot{V}_{De} &= e\left(-\frac{(K+k_{21})}{k_{22}} e - \frac{1}{k_{22}} d\right) \\ &\leq -\frac{1}{k_{22}} |e| \left((K+k_{21})|e| - \sigma\right).\end{aligned} \tag{46}$$

According to (46), $\dot{V}_{De} < 0$ if $|e| > \sigma/(K+k_{21})$. Therefore, the tracking error e is ultimately bounded. ■

REFERENCES

[1] N. P. Reeves and J. Cholewicki, "Modeling the human lumbar spine for assessing spinal loads, stability, and risk of injury," *Crit. Rev. Biomed. Eng.*, vol. 31, no. 1–2, pp. 73–139, 2003, doi: 10.1615/critrevbiomedeng.v31.i12.30.

[2] M. Allegri et al., "Mechanisms of low back pain: A guide for diagnosis and therapy," *F1000Research*, vol. 5, 2016, Art. no. F1000, doi: 10.12688/F1000RESEARCH.8105.1.

[3] R. Bogue, "Exoskeletons – A review of industrial applications," *Ind. Robot*, vol. 45, no. 5, pp. 585–590, May 2018, doi: 10.1108/IR-05-2018-0109.

[4] A. Ali, V. Fontanari, W. Schmoelz, and S. K. Agrawal, "Systematic review of back-support exoskeletons and soft robotic suits," *Front. Bioeng. Biotechnol.*, vol. 9, Nov. 2021, Art. no. 765257, doi: 10.3389/fbioe.2021.765257.

[5] S. Toxiri et al., "Back-support exoskeletons for occupational use: An overview of technological advances and trends," *IISE Trans. Occup. Ergonom. Hum. Factors*, vol. 7, no. 3-4, pp. 237–249, May 2019, doi: 10.1080/24725838.2019.1626303.

[6] RB3D, "L'Exoback," RB3D, Moneteau, France, 2023. [Online]. Available: https://www.rb3d.com/en/exosquelettes/exoback

[7] Germen Bionic, "Cray X," Germen Bionic, Augsburg, Germany, 2023. [Online]. Available: https://germanbionic.com/en/solutions/exoskeletons/crayx/

[8] T. Poliero, V. Fanti, M. Sposito, D. G. Caldwell, and C. Di Natali, "Active and passive back-support exoskeletons: A comparison in static and dynamic tasks," *IEEE Robot. Automat. Lett.*, vol. 7, no. 3, pp. 8463–8470, Jul. 2022, doi: 10.1109/LRA.2022.3188439.

[9] F. Lanotte, L. Grazi, B. Chen, N. Vitiello, and S. Crea, "A low-back exoskeleton can reduce the erector spinae muscles activity during freestyle symmetrical load lifting tasks," in *Proc. IEEE 7th Int. Conf. Biomed. Robot. Biomechatron.*, 2018, pp. 701–706, doi: 10.1109/BIOROB.2018.8488094.

[10] H. K. Ko, S. W. Lee, D. H. Koo, I. Lee, and D. J. Hyun, "Waist-assistive exoskeleton powered by a singular actuation mechanism for prevention of back-injury," *Robot. Auton. Syst.*, vol. 107, pp. 1–9, May 2018, doi: 10.1016/j.robot.2018.05.008.

[11] D. J. Hyun, H. Lim, S. Park, and S. Nam, "Singular wire-driven series elastic actuation with force control for a waist assistive exoskeleton, H-WEXv2," *IEEE/ASME Trans. Mechatron.*, vol. 25, no. 2, pp. 1026–1035, Apr. 2020, doi: 10.1109/TMECH.2020.2970448.

[12] J. won Lee and G. Kim, "Design and control of a lifting assist device for preventing lower back injuries in industrial athletes," *Int. J. Precis. Eng. Manuf.*, vol. 20, no. 10, pp. 1825–1838, 2019, doi: 10.1007/s12541-019-00183-0.

[13] T. Zhang and H. H. Huang, "A lower-back robotic exoskeleton: Industrial handling augmentation used to provide spinal support," *IEEE Robot. Automat. Mag.*, vol. 25, no. 2, pp. 95–106, Jun. 2018, doi: 10.1109/MRA.2018.2815083.

[14] K. Junius, M. Degelaen, N. Lefeber, E. Swinnen, B. Vanderborght, and D. Lefeber, "Bilateral, misalignment-compensating, full-DOF hip exoskeleton: Design and kinematic validation," *Appl. Bionics Biomech.*, vol. 2017, Jul. 2017, Art. no. 5813154, doi: 10.1155/2017/5813154.

[15] S. Toxiri, J. Ortiz, J. Masood, J. Fernandez, L. A. Mateos, and D. G. Caldwell, "A wearable device for reducing spinal loads during lifting tasks: Biomechanics and design concepts," in *Proc. IEEE Int. Conf. Robot. Biomimetic*, 2015, pp. 2295–2300, doi: 10.1109/ROBIO.2015.7419116.

[16] J. D. Sanjuan et al., "Cable driven exoskeleton for upper-limb rehabilitation: A design review," *Robot. Auton. Syst.*, vol. 126, Jan. 2020, Art. no. 103445, doi: 10.1016/j.robot.2020.103445.

[17] A. Mahmoudi Khomami and F. Najafi, "A survey on soft lower limb cable-driven wearable robots without rigid links and joints," *Robot. Auton. Syst.*, vol. 144, Jul. 2021, Art. no. 103846, doi: 10.1016/j.robot.2021.103846.

[18] M. Xiloyannis et al., "Soft robotic suits: State of the art, core technologies, and open challenges," *IEEE Trans. Robot.*, vol. 38, no. 3, pp. 1343–1362, Jun. 2022, doi: 10.1109/tro.2021.3084466.

[19] Y. Mao and S. K. Agrawal, "Design of a cable-driven arm exoskeleton (CAREX) for neural rehabilitation," *IEEE Trans. Robot.*, vol. 28, no. 4, pp. 922–931, Aug. 2012, doi: 10.1109/TRO.2012.2189496.

[20] L. N. Awad et al., "A soft robotic exosuit improves walking in patients after stroke," *Sci. Transl. Med.*, vol. 9, no. 400, Jul. 2017, Art. no. eaai9084, doi: 10.1126/scitranslmed.aai9084.

[21] V. L. Chiu, M. Raitor, and S. H. Collins, "Design of a hip exoskeleton with actuation in frontal and sagittal planes," *IEEE Trans. Med. Robot. Bionics*, vol. 3, no. 3, pp. 773–782, Aug. 2021, doi: 10.1109/tmrb.2021.3088521.

[22] G. Lee et al., "Reducing the metabolic cost of running with a tethered soft exosuit," *Sci. Robot.*, vol. 2, no. 6, May 2017, Art. no. eaan6708, doi: 10.1126/scirobotics.aan6708.

[23] Z. Li, X. Li, Q. Li, H. Su, Z. Kan, and W. He, "Human-in-the-loop control of soft exosuits using impedance learning on different terrains," *IEEE Trans. Robot.*, vol. 38, no. 5, pp. 2979–2993, Oct. 2022, doi: 10.1109/TRO.2022.3160052.

[24] J. Kim et al., "Reducing the metabolic rate of walking and running with a versatile, portable exosuit," *Science*, vol. 365, no. 6454, pp. 668–672, 2019, doi: 10.1126/science.aav7536.
[25] J. Kim et al., "Reducing the energy cost of walking with low assistance levels through optimized hip flexion assistance from a soft exosuit," *Sci. Rep.*, vol. 12, no. 1, 2022, Art. no. 11004, doi: 10.1038/s41598-022-14784-9.
[26] X. Yang et al., "Spine-inspired continuum soft exoskeleton for stoop lifting assistance," *IEEE Robot. Automat. Lett.*, vol. 4, no. 4, pp. 4547–4554, Oct. 2019, doi: 10.1109/LRA.2019.2935351.
[27] Z. Yao, C. Linnenberg, R. Weidner, and J. Wulfsberg, "Development of a soft power suit for lower back assistance," in *Proc. IEEE Int. Conf. Robot. Automat.*, 2019, pp. 5103–5109, doi: 10.1109/ICRA.2019.8794026.
[28] D. A. Quirk et al., "Reducing back exertion and improving confidence of individuals with low back pain with a back exosuit: A feasibility study for use in BACPAC," *Pain Med.*, vol. 24, pp. S175–S186, Jan. 2023, doi: 10.1093/pm/pnad003.
[29] J. Song, A. Zhu, Y. Tu, J. Zou, and X. Zhang, "Cable-driven and series elastic actuation coupled for a rigid–flexible spine-hip assistive exoskeleton in stoop–lifting event," *IEEE/ASME Trans. Mechatron.*, vol. 28, no. 5, pp. 2852–2863, Oct. 2023, doi: 10.1109/TMECH.2023.3235756.
[30] J. M. Li, D. D. Molinaro, A. S. King, A. Mazumdar, and A. J. Young, "Design and validation of a cable-driven asymmetric back exosuit," *IEEE Trans. Robot.*, vol. 38, no. 3, pp. 1489–1502, Jun. 2022, doi: 10.1109/tro.2021.3112280.
[31] S. M. McGill and R. W. Norman, "Partitioning of the l4-l5 dynamic moment into disc, ligamentous, and muscular components during lifting," *Spine*, vol. 11, no. 7. pp. 666–678, Jan. 1986, doi: 10.1097/00007632-198609000-00004.
[32] M. B. Yandell, D. M. Ziemnicki, K. A. McDonald, and K. E. Zelik, "Characterizing the comfort limits of forces applied to the shoulders, thigh and shank to inform exosuit design," *PLoS One*, vol. 15, no. 2, Jun. 2020, Art. no. e0228536, doi: 10.1371/journal.pone.0228536.
[33] R. V. Ham, T. G. Sugar, B. Vanderborght, K. W. Hollander, and D. Lefeber, "Compliant actuator designs," *IEEE Robot. Automat. Mag.*, vol. 16, no. 3, pp. 81–94, Sep. 2009, doi: 10.1109/MRA.2009.933629.
[34] G. A. Pratt and M. M. Williamson, "Series elastic actuators," in *Proc. IEEE/RSJ Int. Conf. Intell. Robots Syst.. Hum. Robot Interact. Cooperative Robots*, 1995, vol. 1, pp. 399–406, doi: 10.1109/iros.1995.525827.
[35] M. C. Sanchez-villamañan, J. Gonzalez-vargas, D. Torricelli, J. C. Moreno, and J. L. Pons, "Compliant lower limb exoskeletons: A comprehensive review on mechanical design principles," *J. NeuroEng. Rehabil.*, vol. 16, no. 55, 2019, Art. no. 55, doi: 10.1186/s12984-019-0517-9.
[36] M. Tiboni, A. Borboni, F. Vérité, C. Bregoli, and C. Amici, "Sensors and actuation technologies in exoskeletons: A review," *Sensors*, vol. 22, no. 3, Jan. 2022, Art. no. 884, doi: 10.3390/s22030884.
[37] J. Lu, K. Haninger, W. Chen, and M. Tomizuka, "Design and torque-mode control of a cable-driven rotary series elastic actuator for subject-robot interaction," in *Proc. IEEE/ASME Int. Conf. Adv. Intell. Mechatron.*, 2015, pp. 158–164, doi: 10.1109/AIM.2015.7222525.
[38] P. Agarwal, J. Fox, Y. Yun, M. K. O'Malley, and A. D. Deshpande, "An index finger exoskeleton with series elastic actuation for rehabilitation: Design, control and performance characterization," *Int. J. Robot. Res.*, vol. 34, no. 14, pp. 1747–1772, 2015, doi: 10.1177/0278364915598388.
[39] T. Chen, R. Casas, and P. S. Lum, "An elbow exoskeleton for upper limb rehabilitation with series elastic actuator and cable-driven differential," *IEEE Trans. Robot.*, vol. 35, no. 6, pp. 1464–1474, Dec. 2019, doi: 10.1109/TRO.2019.2930915.
[40] S. H. Collins, M. B. Wiggin, and G. S. Sawicki, "Reducing the energy cost of human walking using an unpowered exoskeleton," *Nature*, vol. 522, no. 7555, pp. 212–215, Jun. 2015, doi: 10.1038/nature14288.
[41] D. W. Robinson, "Design and analysis of series elasticity in closed-loop actuator force control," Ph.D. dissertation, Dept. Mech. Eng., Massachusetts Inst. Technol., Cambridge, MA, USA, 2000.
[42] H. Vallery, J. Veneman, E. van Asseldonk, R. Ekkelenkamp, M. Buss, and H. van Der Kooij, "Compliant actuation of rehabilitation robots," *IEEE Robot. Automat. Mag.*, vol. 15, no. 3, pp. 60–69, Sep. 2008, doi: 10.1109/MRA.2008.927689.
[43] B. Vanderborght et al., "Variable impedance actuators: A review," *Robot. Auton. Syst.*, vol. 61, no. 12, pp. 1601–1614, Aug. 2013, doi: 10.1016/j.robot.2013.06.009.
[44] S. Wolf et al., "Variable stiffness actuators: Review on design and components," *IEEE/ASME Trans. Mechatron.*, vol. 21, no. 5, pp. 2418–2430, Oct. 2016, doi: 10.1109/TMECH.2015.2501019.
[45] T.-H. Huang et al., "Modeling and stiffness-based continuous torque control of lightweight quasi-direct-drive knee exoskeletons for versatile walking assistance," *IEEE Trans. Robot.*, vol. 38, no. 3, pp. 1442–1459, Jun. 2022, doi: 10.1109/TRO.2022.3170287.
[46] M. Xiloyannis, D. Chiaradia, A. Frisoli, and L. Masia, "Physiological and kinematic effects of a soft exosuit on arm movements," *J. NeuroEng. Rehabil.*, vol. 16, no. 1, 2019, Art. no. 29, doi: 10.1186/s12984-019-0495-y.
[47] W. Cao, C. Chen, H. Hu, K. Fang, and X. Wu, "Effect of hip assistance modes on metabolic cost of walking with a soft exoskeleton," *IEEE Trans. Automat. Sci. Eng.*, vol. 18, no. 2, pp. 426–436, Apr. 2021, doi: 10.1109/TASE.2020.3027748.
[48] H. Yu, S. Huang, G. Chen, Y. Pan, and Z. Guo, "Human-robot interaction control of rehabilitation robots with series elastic actuators," *IEEE Trans. Robot.*, vol. 31, no. 5, pp. 1089–1100, Oct. 2015, doi: 10.1109/TRO.2015.2457314.
[49] H. Liao, H. H. T. Chan, F. Gao, X. Zhao, G. Liu, and W. H. Liao, "Proxy-based torque control of motor-driven exoskeletons for safe and compliant human-exoskeleton interaction," *Mechatronics*, vol. 88, Sep. 2022, Art. no. 102906, doi: 10.1016/j.mechatronics.2022.102906.
[50] L. Liu, S. Leonhardt, and B. J. E. Misgeld, "Design and control of a mechanical rotary variable impedance actuator," *Mechatronics*, vol. 39, pp. 226–236, Jul. 2016, doi: 10.1016/j.mechatronics.2016.06.002.
[51] F. Petit, A. Daasch, and A. Albu-Schaffer, "Backstepping control of variable stiffness robots," *IEEE Trans. Control Syst. Technol.*, vol. 23, no. 6, pp. 2195–2202, Nov. 2015, doi: 10.1109/TCST.2015.2404894.
[52] H. Yu, S. Huang, G. Chen, and N. Thakor, "Control design of a novel compliant actuator for rehabilitation robots," *Mechatronics*, vol. 23, no. 8, pp. 1072–1083, Sep. 2013, doi: 10.1016/j.mechatronics.2013.08.004.
[53] X. Li, Y. Pan, G. Chen, and H. Yu, "Continuous tracking control for a compliant actuator with two-stage stiffness," *IEEE Trans. Automat. Sci. Eng.*, vol. 15, no. 1, pp. 57–66, Jan. 2018, doi: 10.1109/TASE.2016.2574741.
[54] H. Liao, H. H.-T. Chan, F. Gao, X. Zhao, and W.-H. Liao, "Design and characterization of a cable-driven series elastic actuator based torque transmission for back-support exoskeleton," in *Proc. IEEE Int. Conf. Mechatron. Automat.*, 2021, pp. 914–919, doi: 10.1109/ICMA52036.2021.9512715.
[55] P. Dolan, M. Earley, and M. A. Adams, "Bending and compressive stresses acting on the lumbar spine during lifting activities," *J. Biomech.*, vol. 27, no. 10, pp. 1237–1248, Sep. 1994, doi: 10.1016/0021-9290(94)90277-1.
[56] H. H.-T. Chan, H. Liao, F. Gao, X. Zhao, and W.-H. Liao, "A back-support exoskeleton with a cable-driven series-parallel elastic actuation: Prototype design and operational analysis," in *Proc. IEEE Int. Conf. Mechatron. Automat.*, 2021, pp. 206–211, doi: 10.1109/ICMA52036.2021.9512832.
[57] T. R. Waters, V. Putz–Anderson, and A. Garg, "Applications manual for the revised NIOSH lifting equation," DHHS Publ. no. 94-110 (Revised 9/2021), 2021, doi: 10.26616/NIOSHPUB94110revised092021.
[58] F. Lanotte, Z. McKinney, L. Grazi, B. Chen, S. Crea, and N. Vitiello, "Adaptive control method for dynamic synchronization of wearable robotic assistance to discrete movements: Validation for use case of lifting tasks," *IEEE Trans. Robot.*, vol. 37, no. 6, pp. 2193–2209, Dec. 2021, doi: 10.1109/TRO.2021.3073836.
[59] G. Lu et al., "Geographic latitude and human height - statistical analysis and case studies from China," *Arabian J. Geosci.*, vol. 15, no. 4, Feb. 2022, Art. no. 335, doi: 10.1007/s12517-021-09335-x.
[60] A. Middleditch, "Appendix 2 geometric properties of the human body," in *Human Body Dynamics: Classical Mechanics and Human Movement*. Berlin, Germany, Springer, 1999.
[61] J. F. Veneman, R. Ekkelenkamp, R. Kruidhof, F. C. T. Van Der Helm, and H. Van Der Kooij, "A series elastic- and Bowden-cable-based actuation system for use as torque actuator in exoskeleton-type robots," *Int. J. Robot. Res.*, vol. 25, no. 3, pp. 261–281, Mar. 2006, doi: 10.1177/0278364906063829.
[62] P. Guillaume, J. Schoukens, R. Pintelon, and I. Kollái, "Crest-factor minimization using nonlinear Chebyshev approximation methods," *IEEE Trans. Instrum. Meas.*, vol. 40, no. 6, pp. 982–989, Dec. 1991.
[63] L. Ljung., *System Identification Toolbox: User's Guide*. Natick, MA, USA: Mathwork Incoporated, 2023.
[64] A. V. Alexandrov, A. A. Frolov, and J. Massion, "Biomechanical analysis of movement strategies in human forward trunk bending. I. modeling," *Biol. Cybern.*, vol. 84, no. 6, pp. 425–434, 2001, doi: 10.1007/PL00007986.
[65] M. Abdoli-Eramaki, J. M. Stevenson, S. A. Reid, and T. J. Bryant, "Mathematical and empirical proof of principle for an on-body personal lift augmentation device (PLAD)," *J. Biomech.*, vol. 40, no. 8, pp. 1694–1700, Sep. 2006, doi: 10.1016/j.jbiomech.2006.09.006.

[66] M. B. Näf, A. S. Koopman, S. Baltrusch, C. Rodriguez-Guerrero, B. Vanderborght, and D. Lefeber, "Passive back support exoskeleton improves range of motion using flexible beams," *Front. Robot. AI*, vol. 5, Jun. 2018, Art. no. 72, doi: 10.3389/frobt.2018.00072.

[67] M. Schwartz, K. Desbrosses, J. Theurel, and G. Mornieux, "Using passive or active back-support exoskeletons during a repetitive lifting task: Influence on cardiorespiratory parameters," *Eur. J. Appl. Physiol.*, vol. 122, pp. 2575–2583, 2022, doi: 10.1007/s00421-022-05034-x.

[68] C. Di Natali, S. Toxiri, S. Ioakeimidis, D. G. Caldwell, and J. Ortiz, "Systematic framework for performance evaluation of exoskeleton actuators," *Wearable Technol.*, vol. 1, 2020, Art. no. e4, doi: 10.1017/wtc.2020.5.

[69] J. H. van Dieën, "Effects of antagonistic co-contraction on differences between electromyography based and optimization based estimates of spinal forces," *Ergonomics*, vol. 48, no. 4, pp. 411–426, Mar. 2005, doi: 10.1080/00140130512331332918.

[70] T. Kermavnar, A. W. de Vries, M. P. de Looze, and L. W. O'Sullivan, "Effects of industrial back-support exoskeletons on body loading and user experience: An updated systematic review," *Ergonomics*, vol. 64, no. 6, pp. 685–711, Mar. 2021, doi: 10.1080/00140139.2020.1870162.

[71] S. Hwang, Y. Kim, and Y. Kim, "Lower extremity joint kinetics and lumbar curvature during squat and stoop lifting," *BMC Musculoskelet. Disord.*, vol. 10, Feb. 2009, Art. no. 15, doi: 10.1186/1471-2474-10-15.

[72] M. M. Alemi, J. Geissinger, A. A. Simon, S. E. Chang, and A. T. Asbeck, "A passive exoskeleton reduces peak and mean EMG during symmetric and asymmetric lifting," *J. Electromyogr. Kinesiol.*, vol. 47, pp. 25–34, May 2019, doi: 10.1016/j.jelekin.2019.05.003.